EFFECT OF REALISTIC BOUNDARY CONDITIONS ON THE BEHAVIOUR OF CROSS-LAMINATED TIMBER ELEMENTS SUBJECTED TO SIMULATED BLAST LOADS

by

Dominic Cote

Thesis submitted in partial fulfillment of the requirements for the degree of

Master of Applied Science

in Civil Engineering

Under the auspices of the Ottawa-Carleton Institute for Civil Engineering

uOttawa

University of Ottawa

October 2017

ABSTRACT

Cross-laminated timber (CLT) is an emerging engineered wood product in North America. Past research effort to establish the behaviour of CLT under extreme loading conditions has focussed CLT slabs with idealized simply-supported boundary conditions. Connections between the wall and the floor systems above and below are critical to fully describing the overall behaviour of CLT structures when subjected to blast loads. The current study investigates the effects of "realistic" boundary conditions on the behaviour of cross-laminated timber walls when subjected to simulated out-of-plane blast loads.

The methodology followed in the current research consists of experimental and analytical components. The experimental component was conducted in the Blast Research Laboratory at the University of Ottawa, where shock waves were applied to the specimens. Configurations with seismic detailing were considered, in order to evaluate whether existing structures that have adequate capacities to resist high seismic loads would also be capable of resisting a blast load with reasonable damage. In addition, typical connections used in construction to resist gravity and lateral loads, as well as connections designed specifically to resist a given blast load were investigated.

The results indicate that the detailing of the connections appears to significantly affect the behaviour of the CLT slab. Typical detailing for platform construction where long screws connect the floor slab to the wall in end grain performed poorly and experienced brittle failure through splitting in the perpendicular to grain direction in the CLT. Bearing type connections generally behaved well and yielding in the fasteners and/or angles brackets meant that a significant portion of the energy was dissipated there reducing the energy imparted on the CLT slab significantly. Hence less displacement and thereby damage was observed in the slab. The study also concluded that using simplified tools such as single-degree-of-freedom (SDOF) models together with current available material models for CLT is not sufficient to adequately describe the behaviour and estimate the damage. More testing and development of models with higher fidelity are required in order to develop robust tools for the design of CLT element subjected to blast loading.

ACKNOWLEDGEMENTS

Throughout the years of my master's, the arduous tasks involved in completing my research and thesis have allowed me to grow substantially, both as a person as well as a student and member of society. The dedication and patience required over the course of my graduate studies will stay with me in my future endeavours. That being said, I could not have accomplished this feat without the help of several individuals and organizations.

First and foremost, I would like to extend my appreciation to my supervisor and mentor, Dr. Ghasan Doudak, without whom the completion of my thesis would not have been possible. Whether it is through the resources provided, the knowledge imparted onto me or the time invested in helping me with my research, I cannot express enough my gratitude for all the support and guidance he has provided me throughout the years I have known him.

I would also like to take this opportunity to thank the Province of Ontario (OGS) and the University of Ottawa for the financial support which has allowed me to pursue my research with the attention required. Additionally, thank you to Nordic Engineered Wood for providing the material used throughout this study.

Thank you wholeheartedly to the group of individuals who have helped me through the years to complete my research and for their support, namely Ms. America Lopez-Molina, Mr. Christian Viau and Mr. Mathieu Poulin. I would like to acknowledge Mr. Daniel Lacroix for his help and guidance regarding my research and all aspects of my graduate studies.

Last and certainly not least, I would like to thank my mother, father, two brothers and sister for all the support they have provided. Needless to say, I could not have done this without each and every one of you. Thank you for everything.

TABLE OF CONTENTS

LIST OF TABLES

LIST OF FIGURES

NOTATIONS

Acronym		Definition
CLT	=	Cross-laminated timber
DIF	=	Dynamic increase factor
FEA	=	Finite element analysis
LSL	=	Laminated strand lumber
LVDT	=	Linear variable displacement transducer
MDOF	=	Multi-degree-of-freedom
MOE	=	Modulus of elasticity
MOR	=	Modulus of rupture
MSR	=	Machine stress rated
OSB	=	Oriented-strandboard
P-I	=	Pressure-impulse
PSL	=	Parallel strand lumber
SDOF	=	Single-degree-of-freedom
SEA Hut	=	Southeast Asia Hut
TNT	=	Trinitrotoluene

Symbol		Definition
$\phi(x)$	=	Shape function
$(Pmax)_{Avg}$	=	Average applied load at failure
$(PXe)_{Avg}$	=	Average elastic deflection limit
$(Xmax)_{Avg}$	=	Average elastic deflection at failure
$\dot{\varepsilon}$	=	Strain rate
$\bar{m}(x)$	=	Distributed mass per length
$\ddot{y}$	=	Acceleration
μ	=	Ductility ratio
A	=	Loaded area
c	=	Damping constant
$d_{max\text{-}avg}$	=	Average maximum experimental mid-span displacement
F	=	Total load
F(t)	=	Total external force as a function of time
I^-	=	Negative impulse
I^+	=	Positive impulse
I_R	=	Experimental reflected impulse
k	=	Spring constant or stiffness
K_L	=	Load transformation factor
K_{LM}	=	Load-mass transformation factor
K_M	=	Mass transformation factor
K_R	=	Resistance transformation factor
L	=	Clear span length
L_D	=	Driver length
m	=	Mass

$P(t)$	=	Pressure-time history
P_o	=	Ambient pressure
P_R	=	Experimental reflected pressure
P_S	=	Incident peak pressure
$R(t)$	=	Total internal force as a function of time
$R(y)$	=	Non-linear resistance term
t	=	time
t_a	=	Time of arrival of shock wave
t_d	=	Positive phase duration of explosion
t_d^-	=	Negative phase duration of explosion
X_e	=	Deflection at elastic limit
x_{max}	=	Maximum deflection
X_{max}		Deflection at failure
y	=	Displacement
$\dot{y}$	=	Velocity
y_o	=	Initial displacement
$\dot{y}_o$	=	Initial velocity
ω	=	Circular frequency

CHAPTER 1 - Introduction

1.1 Background

Blast is the most unpredictable type of loading and is known to cause severe structural damage and loss of life. The effect of blast loads on the performance of structural members has steadily been gaining interest in the research community due to deliberate attacks and accidental explosions in the past couple of decades. Examples of such events include the attack on the World Trade Center in 2001 and the Oklahoma Bombing in 1995. The majority of research has focused on the behaviour of reinforced concrete and steel due to their inherent blast resisting properties (e.g. mass, stiffness, ductility) and several guidelines and codified provisions have been proposed and enacted in various blast design standards (USADD, 2008; UFC, 2008; FEMA, 2017). These provisions typically include loading, analysis type, and guidance on design and detailing. The Canadian Standard Association has also developed a standard that provides guidance on the analysis and design of structures subjected blast loading, where wood is included as a material option (CSA 2012).

The increasing interest in developing and utilizing massive wood panels in construction and the advancement in technology to produce high performance connections has pushed the boundaries for what can be achieved in timber construction. Mass timber panels (such as cross laminated timber or CLT) have significantly higher mass and stiffness than typical light frame wood systems and their potential for use in blast application has not been thoroughly explored.

1.2 Research Needs

There have been many advancements in the field of timber engineering in recent years. For instance, the provinces of British-Columbia and Ontario enacted provisions that allow for the construction of midrise structures (up to six storeys) to be built entirely out of timber (Government of BC, 2009; Government of Ontario, 2014). Recently, the timber design standard (CSA, 2014) included design and detailing of cross-laminated timber (CLT), which will help facilitate the design and construction of timber buildings in the range of 12-20 storeys in height (e.g. Origine, Brock Commons student residence).

Despite the meticulous effort to produce complete design requirements for CLT panels under gravity as well as wind and seismic loading, no information on how to design such massive panels for blast loading exist. Recent research efforts at the University of Ottawa has established key dynamic characteristics of CLT including strength increase factor (SIF) and dynamic increase factor (DIF), both of which are key parameters used in design and research to develop suitable material predictive models (Poulin et al., 2017). Although the available knowledge has significantly contributed to understanding the behaviour of the material, the study was conducted on CLT slabs with idealized simply-supported boundary conditions. Connections between the wall and the floor systems above and below are critical to fully describing the overall behaviour of CLT structures when subjected to blast loads. The end conditions used in the construction of cross-laminated timber structures may affect the failure mode of the elements or fail prematurely; preventing the wall element from reaching its intended maximum flexural capacity.

The current study investigates the effects of "realistic" boundary conditions on the behaviour of cross-laminated timber walls when subjected to simulated out-of-plane blast loads. Both typical connection details as well as connections that are expected to perform well under blast loading are evaluated experimentally.

1.3 Cross-Laminated timber

Cross-laminated timber (CLT) was initially developed in Austria and Germany and has recently become one of the most promising engineered wood products emerging in the North American market. CLT panels are used in construction of primarily mid-rise structures and are implemented as both walls and floors. Due to the process of pre-fabrication, CLT allows for quick and cost-effective erection producing floors and walls that are massive and behave significantly different than typical light frame wood construction abundantly found in the North American landscape.

CLT panels consist of layers of wood boards that are finger-jointed together and that may be edge glued. These layers are stacked and glued orthogonally to each other to produce large dimension slabs. The boards dimensions vary from 10mm to 50mm in thickness, 60mm to 240mm in width, and are glued together using structural adhesive, although

nails may also be used. Boards may be both visually graded or machine-stress rated and are kiln dried prior to assembly of the panels. The produced panels vary in size, generally ranging from 0.6m to 3m in width, up to 18m in length, and up to 0.4m in thickness.

Although the outer layers of the CLT panels are generally oriented parallel to vertical loads (maximizing wall capacity) or parallel to major span direction in floors (maximizing bending capacity), the orthogonal nature of the slabs provide CLT two-way action capacity. Additionally, the cross-lamination of the layers increases splitting resistance, which is especially beneficial for connection detailing (FPInnovations, 2011). An illustration of a typical cross-laminated timber panel is shown in Figure 1.1.

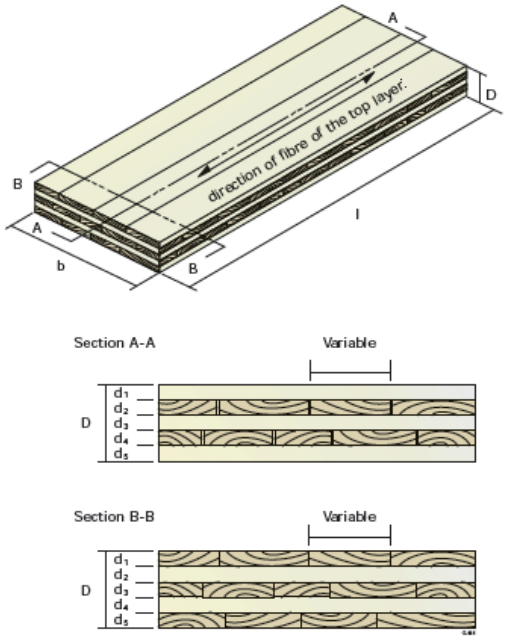

Figure 1.1: Typical CLT Panel Cross-Sections (FPInnovations, 2011)

1.4 Blast Loading

1.4.1 Types of Blast Loading

Explosions occur when a large amount of energy is suddenly released, resulting in a shockwave. This shockwave occurs when the fuel source (in solid or liquid state) turns into gas. Explosions may also be accompanied by radiation and fragmentation depending on the energy source (Dusenberry, 2010).

In addition to the energy source, there are other factors that affect the impact an explosion has on a structural element. One key parameter is the energy release mechanism, namely deflagration or detonation. Deflagration results from volatile explosives gases and occurs when the burning process is subsonic (slower than the speed of sound). These explosions result in lower magnitude shockwaves, requiring additional fuel sources to propagate. Alternatively, detonations are a result of high explosives such as TNT of nitroglycerin reacting with a burning rate that exceeds the speed of sound (known as supersonic). These explosions result in more powerful shockwaves than deflagration and are hazardous to structures. Detonation explosions do not require additional fuel sources to propagate since the energy required is present at the initial explosion.

In addition to the chemical variables which modify the behaviour and impact of a blast load on a structure, physical variables also play a key role in blast loading. Explosions may occur at different distances from the structure in question, different sized explosives, and there may be obstacles between the blast and the structure. Consequently, the intensity with which the blast front (or shockwave) hits may vary and the shape with which the shock front reaches the structure may change. Additionally, the initial blast may occur on the ground causing the blast to spread hemi-spherically or it may occur above ground, resulting in a spherical shockwave (Dusenberry, 2010). Finally, if the explosion takes place in a confined space such as the inside of a building, the effects of deflagration may be equally as destructive as the detonation.

For the purpose of this study, an emphasis will be placed on far-field detonations where the blast would hit the structure with a flat shock front.

1.4.2 Shockwave Characteristics

Following a detonation, the shock front propagates in all directions and reduces in intensity (or pressure) over distance and time. The incident pressure (the initial wave that hits the structure) is increased in magnitude due to the continuous arrival of air particles being pushed by the blast. This increased pressure is called the reflected pressure which is the peak pressure seen by the structure and marks the beginning of the positive phase of the loading. Over time, the compressed air particles expand, reducing the pressure until ambient or atmospheric pressure is reached. This occurs in a time t_d, which is the positive

phase duration. The air particles continue to expand, reducing the pressure even more, which creates a vacuum or negative pressure. This is known as the negative phase and it lasts until the ambient pressure is attained again. This cycle continues until the pressure acting on the structure balances out at ambient pressure. Figure 1.2 shows the different pressure phases following a detonation up to the end of the first negative pressure phase. Although each of the different phases of the time-pressure history have an effect on the structure, all but the initial positive phase are usually ignored in design and analysis since the positive phase typically has the greatest effect on the structure (Dusenberry, 2010). However, this may not be suitable for elements which have been designed solely for unidirectional loading such as window anchors.

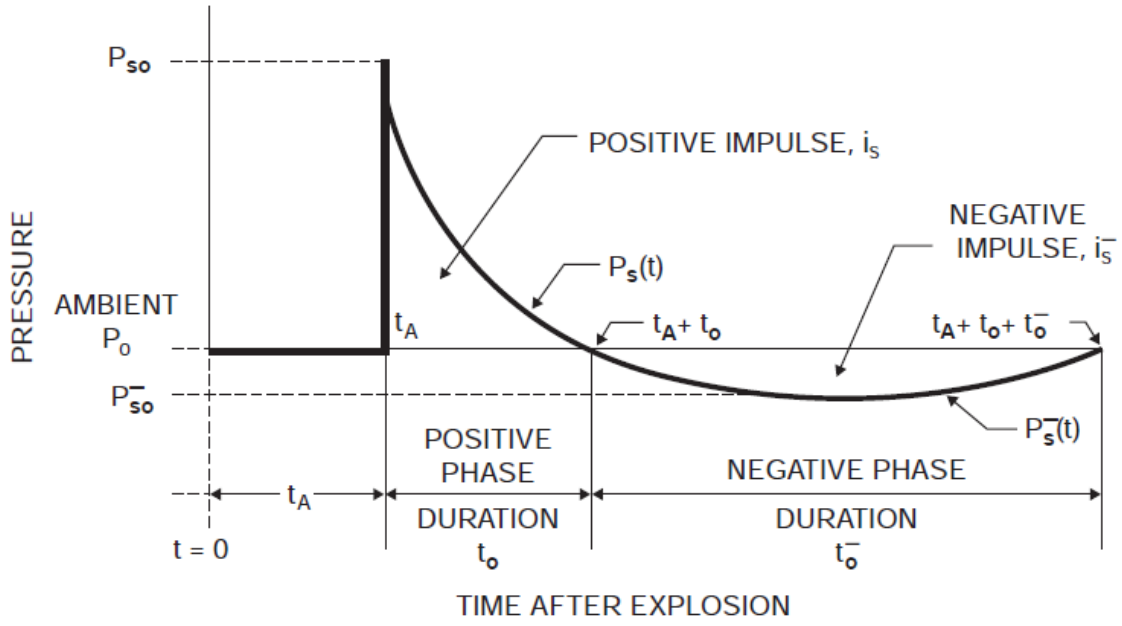

Figure 1.2: Shock Wave from Detonation (Dusenberry, 2010)

For analysis and design purposes, simplifications to the time-pressure history may be made. The initial reflected pressure could be idealized as an instantaneous rise to peak pressure at time zero, after which it decreases linearly until it reaches zero. This simplified pressure-time relationship can easily be plotted allowing the designer to obtain two key design parameters: peak reflected pressure and positive impulse. Impulse is found by calculating the area under the time-pressure curve and is a representation of the energy imparted on the structure by the shockwave. This is done by taking the integral of

the pressure-time history curve from the initial peak, at t_0, to the point of interest, at time t_0+t, as shown in Equation 1.1:

$$I = \int_{t_0}^{t_0+t} P_s \, dt \qquad \text{Equation 1.1}$$

1.5 Dynamic Analysis Methods

1.5.1 Overview

Blast loads are applied over a very short time, and therefore the inertia forces must be accounted for in the analysis and design of the structural elements. Typically, simplified dynamic analysis such as single-degree-of-freedom (SDOF) models are used which account for the kinetic energy and internal forces developed in dynamic loading cases. Key features of this analysis method are highlighted next.

1.5.2 Closed-Form SDOF Analysis

Single-degree-of-freedom (SDOF) models are used to simplify structural elements and facilitate the analysis process of dynamic loading on that element. These models describe the behaviour of the entire element by that of a representative point (e.g. flexural failure of a beam could be described by the mid-span deflection). When the behaviour of an element is not describable by the motion of a single point, a multi-degree-of-freedom (MDOF) model may be used.

When modeling a system as a SDOF, the closed form solution is found by solving the differential equation known as the equation of motion (Eq. 1.2):

$$m\ddot{y} + c\dot{y} + ky = F(t) \qquad \text{Equation 2.2}$$

where $\ddot{y}$, $\dot{y}$, and y are the acceleration, velocity and displacement of the system, respectively.

It is important to note that in blast, damping is considered negligible (Biggs, 1964) since the load duration is short and only the maximum dynamic response is of interest. Assuming the loading function, $F(t)$, can be represented as a triangular pressure-time

history, the response of the system may be described with the following closed-form solution of the equation of motion (Equation 1.3):

$$y(t) = \frac{F_0}{k}(1 - \cos(\omega t)) \qquad \text{Equation 3.3}$$

where F_0 is the peak reflected pressure and ω is the natural frequency of the system in rad/sec.

As mentioned previously, this method assumes that the motion is defined at a given point of interest, and that the mass and stiffness of the system are lumped at that point. This is erroneous since structural elements have distributed mass and stiffness, and must therefore be transformed into an equivalent SDOF system. To do so, transformation factors for the mass, K_m, resistance, K_R, and load, K_L, must be determined and included in the equation of motion. For a simply supported beam deflecting and vibrating according to the first mode shape (maximum deflection at the mid-span), the following transformation factors may be calculated by equating kinetic energy, potential energy and work done by the force applied to the structural system:

$$K_M = \frac{\int_0^L \bar{m}(x)\emptyset^2(x)dx}{\int_0^L \bar{m}(x)dx} \qquad \text{Equation 4.4}$$

$$K_L = \frac{\int_0^L f(x,t)\emptyset(x)dx}{\int_0^L f(x,t)dx} \qquad \text{Equation 5.5}$$

where $\bar{m}(x)$ is the distributed mass over the length of the element, $\emptyset(x)$ is the shape function, according to the first mode deflected shape, and $f(x,t)$ is the distributed load per unit length at a given time.

Using the transformation factors discussed and removing the damping term (Biggs, 1964), the following alternate equation of motion is found:

$$K_M m\ddot{y}(t) + K_R R(y) = K_L A P_R(1 - \frac{t}{t_d}) \qquad \text{Equation 6.6}$$

where A is the area of the element on which the pressure is acting (loaded area) and P_R is the peak reflected pressure discussed previously.

This relationship may be further simplified by equating K_R to K_L. This is due to the fact that the resistance of the system is the internal forces acting against the load on the specimen. The resistance attempts to counter the load; therefore, both distributions of the load and resistance are similar (USADD, 2008). The relationship is additionally simplified by combining the K_L and K_M factors into one variable, K_{LM}, as defined in equations 1.7 and 1.8:

$$K_{LM} = \frac{K_M}{K_L} \qquad \text{Equation 7.7}$$

$$K_{LM} m\ddot{y}(t) + R(y) = AP_R(1 - \frac{t}{t_d}) \qquad \text{Equation 8.8}$$

1.6 Research Objectives

The overall objective of the current research project is to evaluate the behaviour of cross-laminated timber panels with realistic end connections when subjected to simulated blast loads. Specifically, the goals of this project are to:

1) Investigate the effects of connections on the failure mode of the CLT elements;
2) Determine if typical connection detailing for gravity and lateral loads are suitable for blast resistant design of wall elements;
3) Investigate alternative CLT connection detailing for improved blast resistant performance;
4) Evaluate the validity of simplified analysis to predict the deflection behaviour of CLT panels with connection detailing, and;
5) Determine the suitability of CSA S850 standard regarding connections provisions.

1.7 Scope

The objectives mentioned in Section 1.6 are achieved through the implementation of the following steps:

- Perform a thorough literature review on the behaviour of CLT subjected to out of plane loading. Emphasis is put on failure modes under static and dynamic loading;

- Experimentally investigate CLT panels with typical boundary conditions using the University of Ottawa shock-tube and assess their failure modes;
- Investigate possible improvements to typical CLT connection detailing;
- Assess suitability of simplified predictive models by comparing analytical solutions to those obtained experimentally;
- Verify the suitability of current code provisions, and;
- Discuss results, modeling techniques and code implications and suggest improvements to current provisions where applicable.

1.8 Structure of Thesis

Chapter 1 presents an introduction to blast loads and cross-laminated timber, discusses research needs and presents the objectives of the research project.

Chapter 2 presents a literature review of studies that have focused on dynamic behaviour of structural elements, specifically those made of timber or CLT panels, and analytical modeling of wood specimens subjected to blast loads.

Chapter 3 presents an overview of the experimental program, test setup and test specimens investigated.

Chapter 4 presents the experimental results of the dynamic tests performed on CLT panels with typical and modified connection details.

Chapter 5 discusses the experimental and analytical results and highlights key observations on the performance of the various connection types tested. The chapter also presents the implications of this research project on the current code provisions.

Chapter 6 presents a summary of the key findings of this research project and proposes future work to address unanswered questions.

The Appendix presents detailed summaries of the dynamic test results and analysis.

CHAPTER 2 - Literature Review

2.1 Behaviour of Wood under Impact Loading

Early research performed on wood properties focussed on small test specimens that were free of defects and therefore were not representative of the in-situ properties of wood used in industry. Tests were conducted at the Forest Products Laboratory, studying the effects of high loading rate on the compressive and bending strength of wood members (Liska, 1950). The behaviour of defect free wood samples with straight grain were investigated in time durations ranging between 0.3 – 750 s. A compressive and flexural strength increase between 10 – 40% was observed as the time to maximum load decreased. No significant effect was found on the modulus of elasticity. During the in-grade testing it was determined that only full scale tests can adequately reflect the behaviour of wood members due to the presence of defects in the wood (Barrett and Lau, 1994).

Impact tests on defect free specimens were also conducted by Nadeau and Bennett (1982), in order to investigate the effects of rate of loading on the strength of the material. A notch was intentionally cut on the tension face of half of the test specimens in order to study the effect of initial cracks and defects on the behaviour of the member. Strength increase between 10 – 30%, depending on strain rate, was observed for the notch-free test specimens, but this was absent in the weaker test specimens which tend to have initial micro-cracks. The quality of wood and its effect on the variation of strain rate dependency was studied by Jansson (1992). The study concluded that a dynamic strength increase was typically observed in higher quality wood specimens. It was found that poorer quality specimens with knots and cracks would likely fail at the location of the imperfection. Additionally, it was determined that as the time to failure decreased, failure shifted from a crack dependent failure to a harsh break through the specimen.

Sukontasukkul et al. (2000) performed impact loading tests on parallel strand lumber (PSL). Due to the nature of PSL, two failure modes were observed: flexural failure on the tension face and shear failure (or delamination) at the interface between laminates. An average dynamic strength increase of 30% was observed at an approximate strain rate of

3.1 s^{-1}. It was also noted that a decrease in bending strength occurred due to crushing of wood fibers as the impact hammer hit the test specimen.

2.2 Behaviour of Wood Structures under Simulated and Actual Blast Loads

Comparing the quantity of research and information available for high strain rate loading of materials such as steel and concrete to those of wood, it becomes obvious that research on wood structural members under the effect of blast loading is at its infancy. This section summarizes key findings obtained in this area while identifying gaps in research that led to the need for the current study.

2.2.1 Coated Structural Lumber and Laminated Strand Lumber

Tests on coated structural lumber (CSL) and laminated strand lumber (LSL) were conducted during the development of the *Vehicle Bomb Mitigation Guide* (USAF, 2006) as these materials were used in the South-East Asia huts. In an attempt to reduce debris and facilitate repairs following a blast, full scale tests on CSL shelters were performed. The reinforcement of the studs caused the failure to occur in the connections between the wall and floor or roof panels. Uncoated LSL was chosen as a possible alternative to strengthen key locations in the wall (Syron, 2010). High strain rates in the range of $1E^{-5}$ – $1E^{-3}$ s-1 were generated and a dynamic strength increase of 1.31 to 1.37 was observed for the longitudinal direction, while increases of 1.16 to 1.41 was found for the transverse direction.

2.2.2 Shocktube Testing of Individual Wood Studs

A study on the behaviour visually graded wall studs subjected to simulated blasts was performed using the University of Ottawa shocktube was undertaken (Jacques et al., 2013). The study aimed at determining the increase in material properties of specimens subjected to high strain-rate loading. The results from the static and dynamic tests performed in this study were compared in order to determine the increase factor for material properties. For strain rates in the range of 0.1 – 1.0^{-1}, an average dynamic increase factor for the modulus of rupture (MOR) was found to be 1.41. Similarly, an average increase of 1.14 for the modulus of elasticity (MOE) was found, however this increase was found to be insignificant due to the large variability in results and given the small sample size. SDOF modelling showed that this simple tool could accurately predict

the behaviour of wood studs. It was concluded that a linear-elastic resistance curve was able to capture the behaviour of individual wood studs subjected to blast loads.

2.2.3 Shocktube Testing of Light-Frame Stud Walls

Full scale static and dynamic tests on wall systems were performed and the results were compared to determine the DIF for both MOE and MOR (Lacroix and Doudak, 2014). Conducted at a strain rate range of $0.12 – 0.55\ s^{-1}$, this study yielded an average dynamic increase factor for modulus of rupture of 1.40 and for the modulus of elasticity of 1.18. The boundary conditions of each test were simply supported to avoid influence of the connections. A material predictive model was developed based on the partial composite action between the sheathing and the stud. The model was capable of predicting the dynamic response of the wall with reasonable accuracy. The mechanical fasteners connecting the sheathing to the framing elements were found to be the main sources of ductility. Comparing the results from several studies including impact tests, Lacroix and Doudak (2014) presented an empirical function to calculate the dynamic increase factor for the modulus of rupture of wood studs.

2.3 Retrofit Options for Light-Frame Wood Stud Walls

Wood is an inherently light and brittle material, which may lead to poor performance under blast loads. Research dealing with the enhancements of the wood performance against blast loads is discussed in this section.

2.3.1 Sheathing Deficiencies and Debris

As blast loads cause significant damage to wood elements, debris and injuries are of concern in blast research. A study on structural and non-structural elements subjected to blast loading was performed using anthropomorphic tests devices (test dummies) to judge injury levels (Bogosian and Avanessian, 2004). This study showed that debris was the main mechanism causing injuries or death in blasts, and a relationship was established between injury levels and pressure-impulse combinations. The study found that wood stud walls could cause moderate to high injury levels, based on the assumption that wood stud walls would fail at the connections, thus striking the test dummies with debris on the chest. The findings emphasized the need for more research on the behaviour of connections and the role they play in affecting the behaviour of the structural elements.

The United States Air Force produced a report describing the results of blast tests on the South-East Asia huts (mentioned in section 2.2.3) with the goal of determining potential retrofit options (USAF, 2006). These huts included window and door openings and were built of dimensional lumber enclosed with plywood. The findings showed that it was not the component and structural damage that would likely cause injury to the occupants but rather structural collapse. The occupants' location relative to the source of the debris also played a significant role. The study suggested that the huts should be retrofitted with additional sheets of plywood on the interior and exterior walls, and that additional dimensional lumber should be placed at the bottom of the walls to prevent failure at the connections.

Lacroix et al. (2013) performed tests on wood stud walls with varying levels of pressure-impulse combinations using the University of Ottawa shocktube. The study concluded that walls with thicker sheathing performed significantly better than those with typical light frame detailing following prescriptive design requirements. It was observed that in some test specimens, walls with typical sheathing thickness often tore prior to the studs failing which resulted in the wall not attaining it full strength. Damage to the thicker sheathing was limited to minor cracking, and the wall studs generally reached their ultimate flexural strength in those test specimens. Retrofits for the studs and wall were also investigated (Lacroix et al., 2013). An increase in capacity and stiffness compared to typical construction detailing was achieved.

Viau and Doudak (2016) investigated the behaviour of wood walls in the region corresponding to hazardous-blowout damage levels. The study confirmed finding by Lacroix et al. (2013) where premature sheathing failure was found to take place prior to attaining the full flexural response of the studs. This failure was mitigated through reinforcement with thicker sheathing and the use of screws instead of nails to connect the sheathing to the studs. This was also found to reduce the amount of debris. Welded wire mesh was successfully used to strengthen the sheathing and as a catcher system. Static material properties of the wall components were determined and used as input in an analytical model that was successfully validated using the experimental test results.

2.3.2 Boundary Connection Deficiencies

Sorensen and McGill (2011) investigated the failure in the connections when stud walls are exposed to blast loading which adds significantly to the debris created since the whole wall may become airborne and possibly strike the occupants. The study found that ensuring the structural integrity of the connections between wall and floors is critical in limiting the risk of injury due to debris in addition to reducing the likelihood of progressive collapse of the structure.

A prototypical retrofit to mitigate deficiencies in connections for light frame stud walls was developed and tested at the University of Ottawa. The retrofit consisted of a hanger type fastener and tensioning rods which would allow for direct connection between the ends of the wall studs and rim-joist members (Lloyd and Jacques, 2011). The retrofit also allowed for an effective load path and assisted in distributing the load into the floor diaphragm. Both typical and retrofitted walls were tested in this study and while the typically built walls failed at the connections as expected, no connection failure in the retrofitted walls was observed.

2.4 Static and Dynamic Modeling of Wood Studs

Research has shown that connection in wood can be assumed as semi-rigid while providing partial composite action between elements. A method that describes the behaviour of sheathed wood floors was developed by simulating the floor as a T-beam (McCutcheon, 1977). The methodology was also followed for the evaluation of stud walls.

Modeling of the dynamic interactions between stud walls, bottom/top plates and structure foundations was conducted using finite element analysis (FEA), where multi-linear material predictive models were used by Polensek and Schimel (1986). The aim of the study was to determine the rotational restraint at the ends of stud walls with typical fastening details. Full-scale stud walls were tested with different end connection details offering different levels of rotational restraint. Although as-built walls exhibited on average 2% rotational restraint, the authors noted that providing additional nailing and extending the diaphragm sheathing past the bottom and top plates provided the system with a 13% support restraint.

Viau and Doudak (2016) investigated the performance of light-frame wood stud walls under simulated blast loading with realistic boundary conditions. The study included connection detailing based on prescriptive requirements for low and high seismic and wind regions. The study also evaluated different connection options to ensure that failure occurred in the stud rather than the connection as specified in the Canadian blast design standard (CSA 2012). The results highlighted the inadequate behaviour of typical prescriptive connection detailing and showed that connections designed specifically for blast performed well. The study also highlighted that basing the connection design solely on capacity may not be adequate.

SDOF modelling was implemented to validate analytical models developed for light frame wood stud walls using experimental results (Lacroix and Doudak, 2013). There was good agreement between the proposed analytical model and the test results.

2.5 Behaviour and Modeling of CLT Panels under Simulated Blast Loads

Cross laminated timber (CLT) has been designed and used in construction in Europe as a proprietary material for twenty years. The recent inclusion of CLT in the Canadian timber design standard (CSA 2014) has highlighted the need for more research on this material for various applications. Several studies has investigated the material properties of CLT, especially rolling shear (e.g. Zhou, et al., 2014; Li and Lam, 2016). The behaviour of CLT subjected to in- and out-of-plane loads has also been studied by several researchers (e.g. Steiger and Gülzow, 2009; Sikora, et al., 2016; Ceccotti, et al., 2006; Popovski and Gavric, 2016; Yasumara el. al., 2016). The investigation of the effect of blast loading on CLT panels has been limited to a demonstration project from the joint efforts of Woodworks USA and the University of Maine (*WCTE, 2016*) and a study conducted at the University of Ottawa (Poulin et al., 2017). The latter is of great interest to the current study since it is, to the author's knowledge, the only study done on CLT panels subjected to simulated blast loading. Also, the material in the current study is a subset of that used in the study by Poulin et al. (2017). The study is therefore described in more details next.

A total of eighteen CLT panels were investigated by Poulin et al. (2017) where three-ply and five-ply panels with panel thicknesses of 105 mm and 175 mm, respectively, were investigated. The aim of the study was to establish failure mechanisms and determine a

dynamic increase factor that can be used in design and modeling of the material. The authors determined the average dynamic increase factor to be 1.28 for resistance, whereas no increase in stiffness was observed. Flexural failure at the mid-span was the prominent failure mode in every test, with rolling shear occurring in the transverse layers. Rolling shear failure was observed prior to or at ultimate failure which was dominated by flexure failure initiated at the finger joints on the tension face. Table 2.1 summarizes the key results for the dynamic test from the study by Poulin et al. (2017). The table presents the reflected pressure (P_R), reflected impulse (I_R), maximum dynamic resistance (R_{Max}), deflection at maximum resistance (Δ_{Rmax}), maximum recorded deflection (Δ_{max}), ductility ratio (μ), time to failure ($t_{f\text{-}max}$), maximum mid-span strain ($\dot{\varepsilon}$), static stiffness (K_{static}) and failure modes.

Table 2.1: Simply Supported 3-Ply CLT Dynamic Test Results (Poulin et al., 2017)

Test name	P_R	I_R	R_{max}	Δ_{Rmax}	Δ_{max}	μ	$t_{f\text{-}max}$	$\dot{\varepsilon}$	K_{static}	Failure mode
	(kPa)	(kPa-ms)	(kN)	(mm)	(mm)		(ms)	(s^{-1})	(kN/mm)	
CLT3-4.1	11.6	90.0		16.1	16.1		26.8	5.00E-02	1.59	Elastic
CLT3-4.2	38.7	379.3	82.1	37.7	105.2	2.8	48.8	1.61E-01	1.59	Rolling shear
CLT3-5.1	48.2	442.3	80.7	40.5	88.6	2.2	25.6	1.44E-01	2.10	Flexural
CLT3-6.1	52.6	613.7	88.3	45.8	143.7	3.1	35.0	1.52E-01	1.88	Flexural
CLT3-7.1	6.5	79.1	-	-	11.8	-	30.6	2.86E-02	1.77	Elastic
CLT3-7.2	52.8	439.9	-	-	119.2	-	47.2	1.58E-01	1.77	Rolling shear
CLT3-8.1	5.8	59.4	-	-	10.1	-	28.0	2.16E-02	1.66	Elastic
CLT3-8.2	49.0	467.7	-	-	89.5	-	26.0	1.79E-01	1.66	Rolling shear, then flexural
CLT3-9.1	12.2	131.2	-	-	18.7	-	31.2	5.22E-02	1.76	Elastic
CLT3-9.2	30.9	322.4	-	-	58.4	-	38.8	1.32E-01	1.76	Rolling shear
CLT3-10.1	9.1	92.6	-	-	12.3	-	26.2	3.61E-02	2.10	Elastic
CLT3-10.2	34.0	374.4	-	-	99.4	-	79.6	1.58E-01	2.10	Flexural
CLT3-11.1	9.2	106.5	-	-	11.7	-	26.5	3.52E-02	2.09	Elastic
CLT3-11.2	32.9	345.4	-	-	72.5	-	35.2	1.19E-01	2.09	Flexural
Average			83.7	41.3	112.5	2.7				
COV			0.04	0.08	0.21	0.14				

Table 2.2: Simply Supported 5-Ply CLT Dynamic Test Results (Poulin et al., 2017)

Test name	P_R	I_R	R_{max}	Δ_{Rmax}	Δ_{max}	μ	$t_{f\text{-}max}$	$\dot{\varepsilon}$	K_{static}	Failure mode
	(kPa)	(kPa-ms)	(kN)	(mm)	(mm)		(ms)	(s^{-1})	(kN/mm)	
CLT5-4.1	53.7	610.4	176.7	32.4	80.7	2.5	34.2	2.05E-01	5.64	Flexural
CLT5-5.1	58.6	690.7	171.7	29.6	58.2	2.0	26.2	1.80E-01	5.14	Rolling shear
CLT5-6.1	7.2	81.7	-	-	6.5	-	22.4	2.56E-02	5.53	Elastic
CLT5-6.2	55.8	602.4	-	-	77.9	-	31.4	2.13E-01	5.53	Flexural
CLT5-7.1	7.3	81.8	-	-	6.4	-	22.8	3.28E-02	5.07	Elastic
CLT5-7.2	51.2	481.2	-	-	37.0	-	24.2	2.12E-01	5.07	Flexural
Average			174.2	31.0	69.5	2.3				
COV			0.01	0.04	0.16	0.11				

Two resistance material predictive models, which account for high strain-rate effects and the experimentally observed post-peak residual behaviour, were developed. A single degree-of-freedom model was validated using full-scale simulated blast load tests, and the predictions were found to match well with the experimental displacement-time histories. Figure 2.1 shows the resistance curves developed for both three-ply and five-ply CLT slabs.

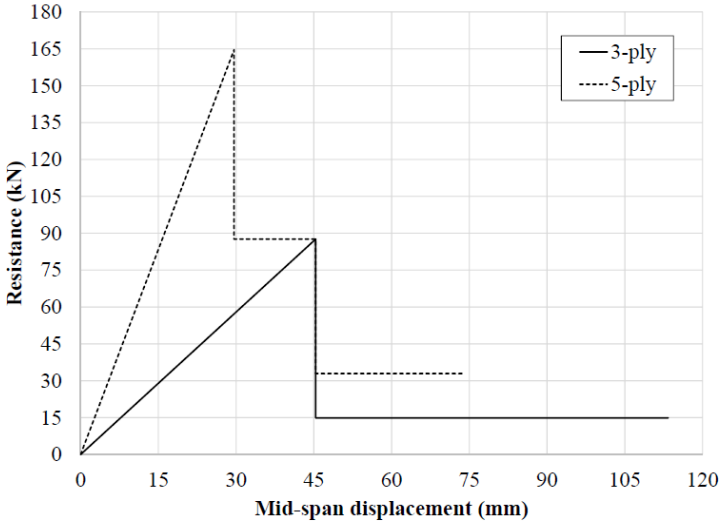

Figure 2.1: Simply Supported CLT Dynamic Resistance Curves (Poulin et al., 2017)

Initial peaks in both the 3-ply and 5-ply resistance curve were found experimentally, and the displacement corresponding to the peak resistance was determined using the measured stiffness during static testing. The drop in resistance for both curves represents the loss of the tension side longitudinal and transverse laminates. This indicates that for 5-ply elements, the initial drop results in the CLT panel to now behave as a 3-ply specimen. At a displacement equal to the elastic limit of 3-ply specimens, the resistance curve drops to 20% of the ultimate 5-ply resistance. This resistance is maintained until a ductility ratio of 2.5 is reached.

As mentioned earlier, the study was limited to idealized boundary conditions which provides essential information on the behaviour of the CLT slabs themselves but lacks the ability to evaluate the performance of actual structures including realistic boundary

connections. This was the main motivator to undertake the work in the current study, as will be described in the following chapters.

CHAPTER 3 - Experimental Program

3.1 Material

As part of the current research project, a total of thirteen dynamic tests were performed on CLT panels with varying connection detailing. This chapter provides a description and summary of the experimental phase of the study.

The dynamic tests were performed on five-layer X-Lam CLT slabs. The motivation behind this choice was consistency in the size, species and grade of the CLT panel in order to allow direct comparisons between various connection types tested. The specimens were comprised of layers of 35mm by 80mm S-P-F with $1950F_b$ machine stress rated lumber used in layers oriented in the major direction and No. 3/Stud lumber in layers oriented in the minor direction. The slabs were manufactured by gluing the five layers perpendicular to each other. This produced 175mm thick slabs, which were cut to a width of 450mm and a length of 2500mm. The length had to be reduced to 2082mm (82 inches) in order to fit in the shocktube apparatus. The slab was connected to two horizontal panel pieces using the connections investigated. This was done to allow the clear span of the tests specimens to fit the test setup and to provide and area to clamp the test specimen to the shocktube (described later in this chapter).

Five different Heco-Topix screws were used to connect the slabs to each other directly or through two different types of steel angles. Three types of screws were used to create various connections types, including 300mm long screws, with 6mm and 8mm in diameter; 120mm long screws, with 8mm and 10mm diameter; and 350mm long double-threaded screws, with 8.5mm diameter. Two steel angle types were used; one consisted of ML24Z steel angles from Simpson Strong-Tie; and the other of 6.6mm thick manufactured steel angle. For some of the configurations, the connections were designed based on the capacity of the CLT slabs. For the purpose of this research project, the designed connections were selected by considering a 20% increase on the dynamic reaction (CSA 2012) obtained from tests on CLT panels with simply-supported boundary conditions obtained from published test results on panels from the same batch as those used in the current research study (Poulin et al., 2017). Specifics on the test slabs and

connection hardware details are shown in Figures 3.1 to 3.8. Table 3.1 and Table 3.2 then summarize the connection hardware and dimensions.

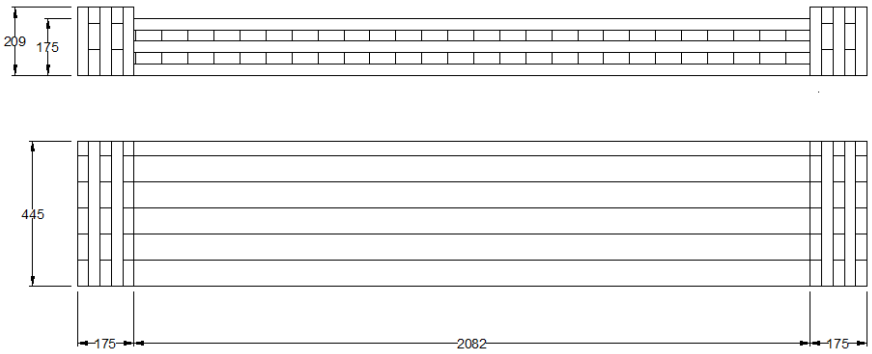

Figure 3.1: Typical Test Specimen (Without Connection Detail)

Figure 3.2: Screw A – 8x120 Heco-Topix Zn Blau

Figure 3.3: Screw B – 10x120 Heco-Topix Zn Blau A2K

Figure 3.4: Screw C – 6x300 Heco-Topix Zn Gelb A2L

Figure 3.5: Screw D – 8x300 Heco-Topix Zn Gelb A2L

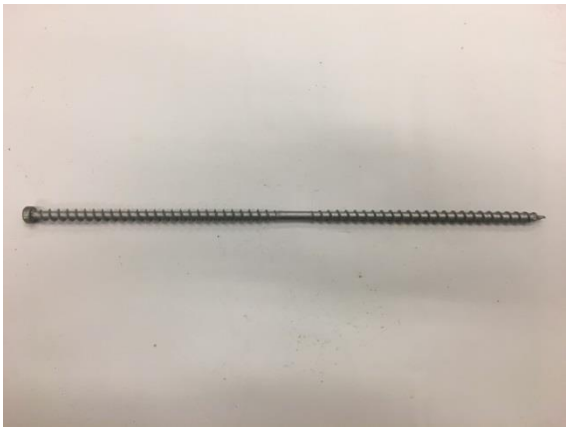

Figure 3.6: Screw E – 8.5x350 ZnA2K+DS-Beschichtet

Figure 3.7: Angle A – ML24Z angle

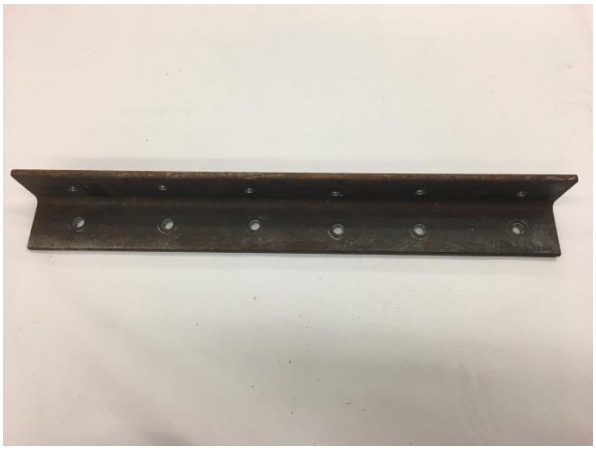

Figure 3.8: Angle B – Stiff Manufactured Angle

Table 3.1: Test Screw Details

	Screw Name	Screw Length (mm)	Threaded Length (mm)	Diameter of Threads (mm)
A	8x120 Heco-Topix Zn Blau	120	70	8.3
B	10x120 Heco-Topix Zn Blau A2K	120	120	10.3
C	6x300 Heco-Topix Zn Gelb A2L	300	70	6.2
D	8x300 Heco-Topix Zn Gelb A2L	300	100	8.3
E	8.5x350 ZnA2K+DS-Beschichtet	350	160 (per threaded portion)	8.7

Table 3.2: Test Angle Details

	Angle Name	Angle Width mm (in)	Angle Height and Depth mm (in)	Thickness mm(in)
A	ML24Z	101.6 (4)	50.8 (2)	2.77 (7/64)
B	Manufactured thick angle	431.8 (17)	50.8 (2)	6.35 (1/4)

Figures 3.9 to 3.10 show the connection details used in the study, and Table 3.3 describes the test matrix for the current experimental program.

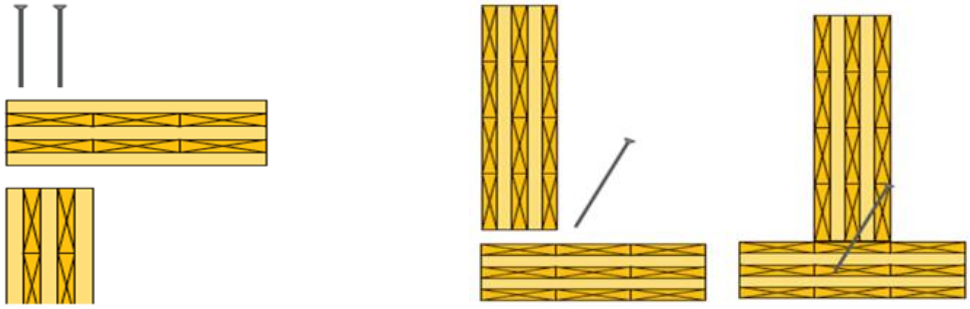

A) End-Grain Screws **B) Double-Threaded Screws**

Figure 3.9: Typical Connection Details

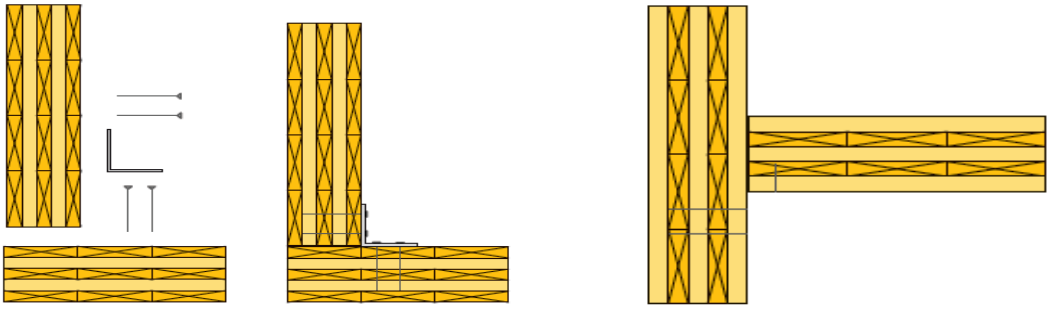

C) Angle Brackets **D) Balloon Construction**

Figure 3.10: Improved Bearing Connection Details

Table 3.3: Experimental Program Summary

Connection Type	Specimen	Bottom Connection Detail	Top Connection Detail
Typical End-Grain Screws	CLT 5-1	• 4 Angle A • 5 Screw A (per angle face)	• 25 Screw C
	CLT 5-2	• 2 Angle A • 3 Screw A (per angle face)	• 12 Screw C • 5 Screw B (reinforcement)
	CLT 5-3	• 27 Screw D • 10 Screw B (reinforcement)	• 27 Screw D • 10 Screw B (reinforcement)
Typical Double-Threaded Screws	CLT 5-4	• 2 Screw E @ 60°	• 2 Screw E @ 60°
	CLT 5-5	• 8 Screw E @ 60°	• 8 Screw E @ 60°
Thin Angle Brackets	CLT 5-6	• 2 Angle A • 3 Screw A (per angle face)	• 2 Angle A • 3 Screw A (per angle face)
	CLT 5-7	• Repeat of CLT 5-6	
	CLT 5-8	• Repeat of CLT 5-6	
	CLT 5-9	• Repeat of CLT 5-6	
Thick Angle Brackets	CLT 5-10	• 1 Angle B • 6 Screw A	• 1 Angle B • 6 Screw A
	CLT 5-11	• Repeat of CLT 5-10	
Balloon Construction	CLT5-12	• Balloon Construction	
	CLT5-13	• Repeat of CLT 5-12	

3.2 Dynamic Testing

This section describes the testing setup and methodology used in the current research study. Testing CLT panels with realistic boundary conditions subjected to simulated blast loads was accomplished using the University of Ottawa's shocktube facility, which is capable of generating pressure waves to simulate far-field detonations created by high explosives.

3.2.1 Description of the Shocktube Facility

The shocktube simulates blast loads by compressing air and releasing it almost instantaneously. This is possible due to the three main components of which the shocktube comprises: the driver section, the diaphragm section, and the expansion chamber. The way the air interacts with a specimen could either be direct if the specimen is produced in the same size as the end frame, or through a load transfer device (LTD) when the test specimen is smaller in width than the end frame. Figures 3.11 to 3.13 show the various components of the shocktube facility.

A safe and predictable double-diaphragm firing mechanism is used to build up and release the pressurized air onto the test specimen. As seen in Figure 3.12, aluminum foils are placed between the driver and diaphragm, as well as between the diaphragm and expansion chamber. The thickness and quantity of foils are selected to produce the desired pressure and ensure that premature trigger does not occur. The driver length can be varied in order to produce different pressure-impulse combinations for each shot. Pressure is built up in the driver section until the desired level is achieved. The pressure in the diaphragm is controlled such that the differential pressure between the driver and diaphragm, as well as between the diaphragm and atmospheric pressure found in the expansion chamber, does not exceed the capacity of the foils in between various sections. Once the desired pressure is reached in the driver, the diaphragm pressure is reduced, causing the difference in pressure between the driver and diaphragm to be more than the foil capacity between these two sections. It is at this point that the foils rupture and the pressure wave travels through the 6096 mm (20 ft) expansion chamber and interacts with the specimens mounted at the end frame. The 2032 x 2032 mm^2 opening of the shocktube allows for the testing of large or full-scale structural elements. The expansion section also

includes vented openings near the end frame, which allow the pressures to escape during the negative phase of the test.

The load transfer device consists of hinged steel panels which allow it to bend out of plane, while transferring the load to the test specimen. Reinforced steel I-beams with welded rollers were implemented such that the load was applied as a four-point bending with the load application points located at the third points of the test specimens (694 mm apart). Based on preliminary analysis, a 2743 mm (9 ft) driver section was found suitable for all the pressure and impulse ranges needed in the current project.

Figure 3.11: Shocktube Driver and Diaphragm Section

Figure 3.12: Shocktube Expansion Chamber

Figure 3.13: Shocktube Load Transfer Device Description of the Test Setup

3.2.1.2 End Connections

The two panel pieces cut from the end of each CLT slab were used to simulate floor diaphragms as part of creating the boundary conditions for the slabs. These end blocks were attached to the slab using the connection detail to be investigated, simulating the connection between a CLT wall and the floors above and below. The test specimen was placed flush against the load application points of the load transfer device. Spacing blocks were positioned under the test specimen to ensure proper alignment with the shocktube opening, such that the third points of the slab were in line with the load application points. The blocks at the ends of the CLT slab were then clamped to the shocktube using hollow steel sections and steels rods protruding from the shocktube's end frame. The spacing blocks were removed to allow for vertical movement, in case the clamped blocks moved or rotated slightly. This end conditions simulates the in-plane stiffness of the floors above and below the CLT wall. A detailed schematic of side and front view of the dynamic test setup are show in Figure 3.14 and 3.15, respectively.

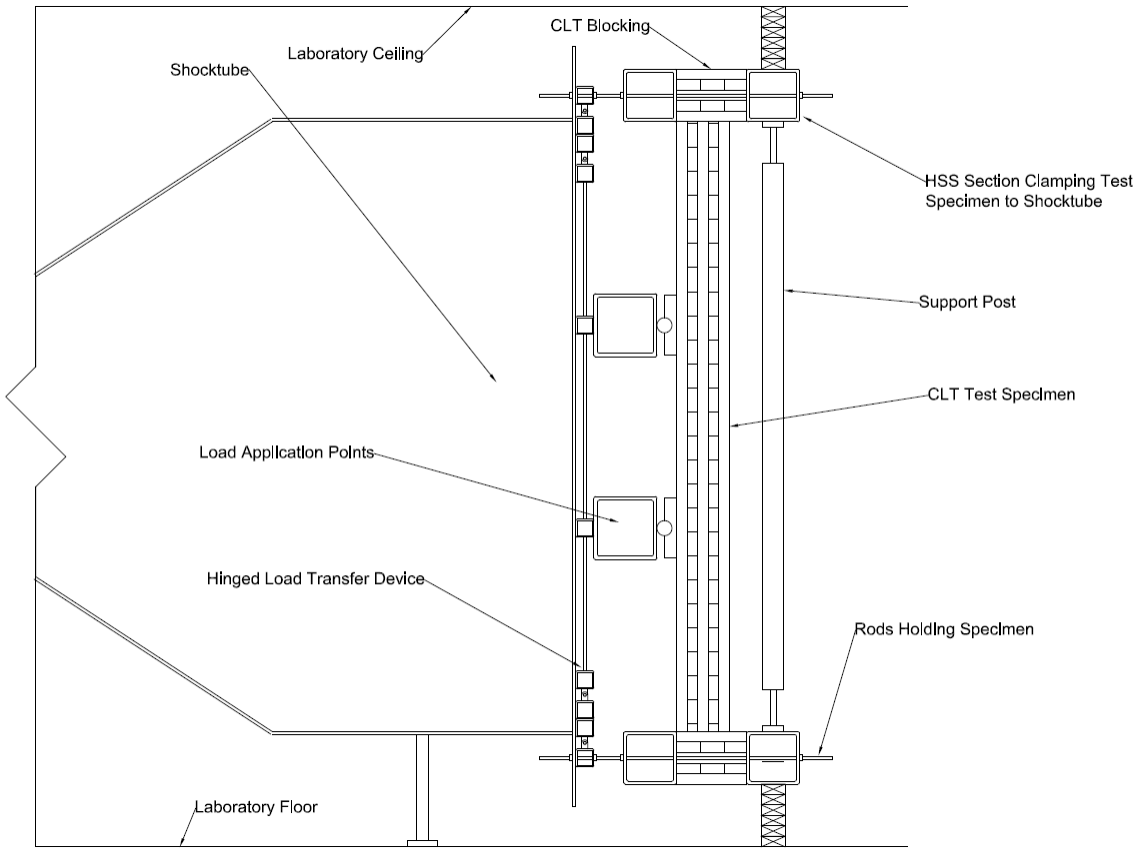

Figure 3.14: Dynamic Test Setup - Side View

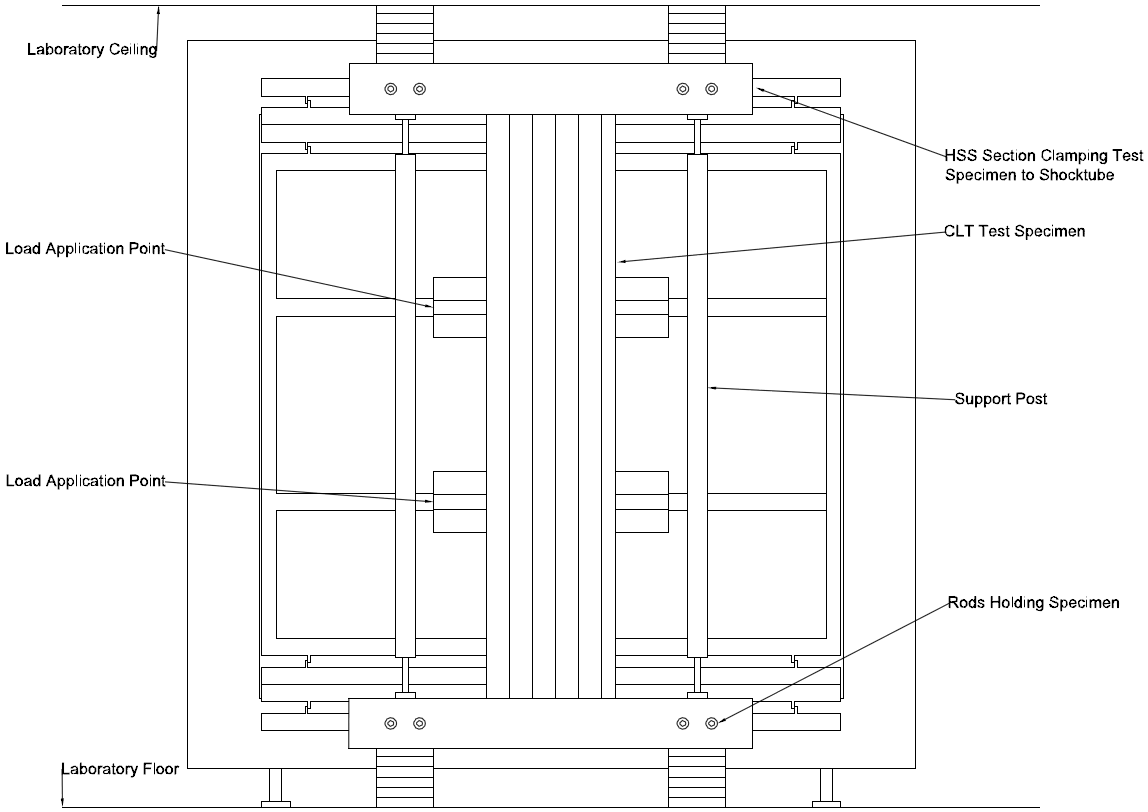

Figure 3.15: Dynamic Test Setup - Front View

3.2.1.3 Measuring Methods and Equipment

To capture the behaviour of the specimens during the investigation, readings of the pressure, displacement, and strain were documented. Also, a high speed camera, recording at a rate of 500 frames per second and with a resolution of 800 x 600 pixels was used to capture the motion of the specimens during the tests. This was essential in order to review the sequence of failures and displacements leading up to the overall failure of the test specimen.

The reflected pressure acting on the CLT slabs was measured using two piezoelectric pressure sensors, located at the side and bottom of the shocktube opening. Once the initial blast wave passed these pressure sensors, the recording of the different devices was triggered. The data acquisition system (DAS) was capable of recording data at 100,000 readings per second continuously for the duration of the test. The slab displacement was measured using 300 mm stroke linear variable displacement transducers (LVDT). The LVDT was attached to a steel post enabled the measurement of the slab deflection at mid-span. To protect the LVDTs, a steel encasement was devised and installed at the steel bracket. This encasement had the goal to protect the LVDT when the deflection of the specimen was larger than the maximum stroke of the LVDT.

Strain on the compression and tension faces of the slab at mid-span was also measured using 350 Ohm strain gauges. The CLT face was sanded and cleaned prior to adhering the strain gauges to the face of the specimens using cyanoacrylate adhesive, shown in Figure 3.16. Typical test setup, including the equipment used, can be seen in Figures 3.17 to 3.18.

A) Packaging

B) Adhesive

Figure 3.16: Cyanoacrylate Adhesive

A) Strain Gauge

B) LVDT

Figure 3.17: Measurement Devices

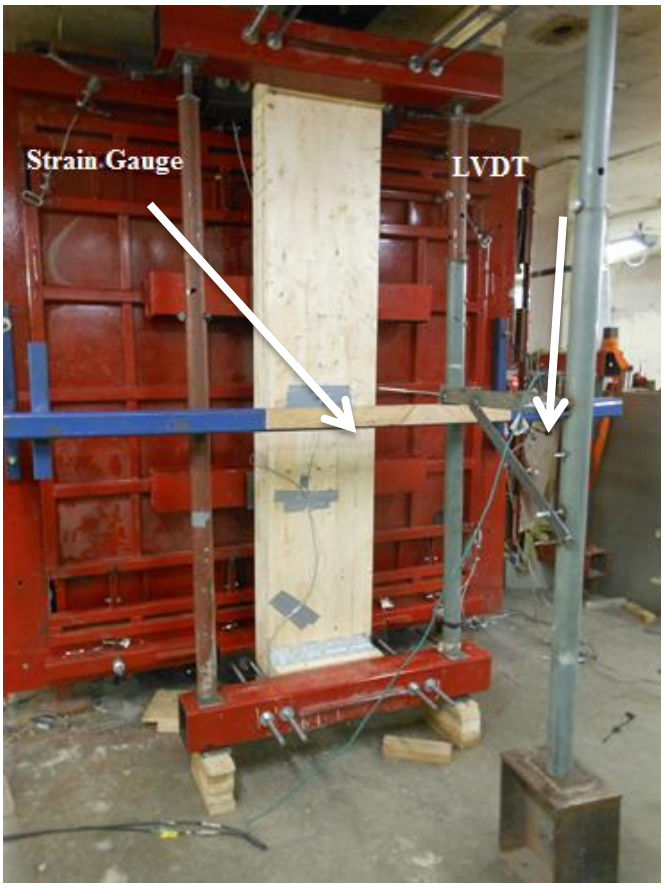

Figure 3.18: Measurement Device Placement

CHAPTER 4 - Experimental Results

4.1 Dynamic Results

This chapter presents the experimental results for the dynamic tests described in Chapter 3. The characteristics of each test specimen are provided in addition to details on the pressure-impulse combinations applied and typical failure modes. A summary of the measurements taken during the tests may be found in Table 4.1 at the end of the chapter, and more information regarding measured pressures and impulses as well as displacement and strain data can be found in Appendix A. With regards to the nomenclature used for each test, CLT 5-X indicates that the tests were performed on five-ply CLT panels, followed by the specimen number. The tests are grouped to reflect typical connection detailing used in gravity or lateral load design with or without reinforcement of joint against perpendicular to grain tension failure (Section 4.2), angled screw connections (Section 4.3), angle brackets with dimensions that allow them to yield (Section 4.4) or thicker angle brackets where yielding is not likely (Section 4.5). Finally, boundary conditions representative of balloon framing were investigated, where some rotational stiffness is expected (Section 4.6)

The connection capacity for each test was based on seismic design considerations in order to evaluate the suitability of such connections to resist blast load or using the blast design standard requirements (CSA 2012). For the connections assumed to be typical in seismic design, the base shear was determined considering a six-storey CLT building, with a 40m by 40m footprint, located in Ottawa, Ontario. The connection capacities were determined based on design level values as required by the standard requirements for seismic design (CSA 2012). For connections designed for blast, the calculations were done by determining the reaction load for similar 5-ply CLT panels measured in previous dynamic tests (Poulin et al. 2017) and then estimating the connection capacity by adding 20% to the attained reaction force as required by the blast design standard (CSA 2012).

4.2 Typical End-Grain Screw Detailing

4.2.1 CLT 5-1

This test configuration consisted of CLT connections typically used in construction to resist gravity loads. The purpose of this test was not only to investigate whether typical connections have any inherent blast resisting capabilities but also to document whether the failure mode is suitable for blast design (i.e. possesses some level of ductility). The joint capacity was calculated using the blast standard requirements. The top connection consisted of twenty-five screws driven straight through the top supporting block (simulating CLT floor slab) and into the end grain of the CLT wall. The fasteners consisted of Heco-Topix Zn Gelb A2L screws, with a diameter of 6 mm and a length of 300 mm. The bottom connection comprised of four ML24Z steel angles (2.77 mm thick L-shaped) representing angle brackets. This joint was fastened using Heco-Topix Zn Blau screws, with a diameter of 8 mm and a length of 120 mm. A total of forty screws (twenty on each side) were used. Figure 4.1 displays the top and bottom connections for this test.

A) Top Connection **B) Bottom Connection**

Figure 4.1: CLT 5-1 Connection Details

Figure 4.2 shows the applied pressure-impulse combination while Figure 4.3 shows the deflection and strain time histories. Complete details for all tests can be found in Appendix A.

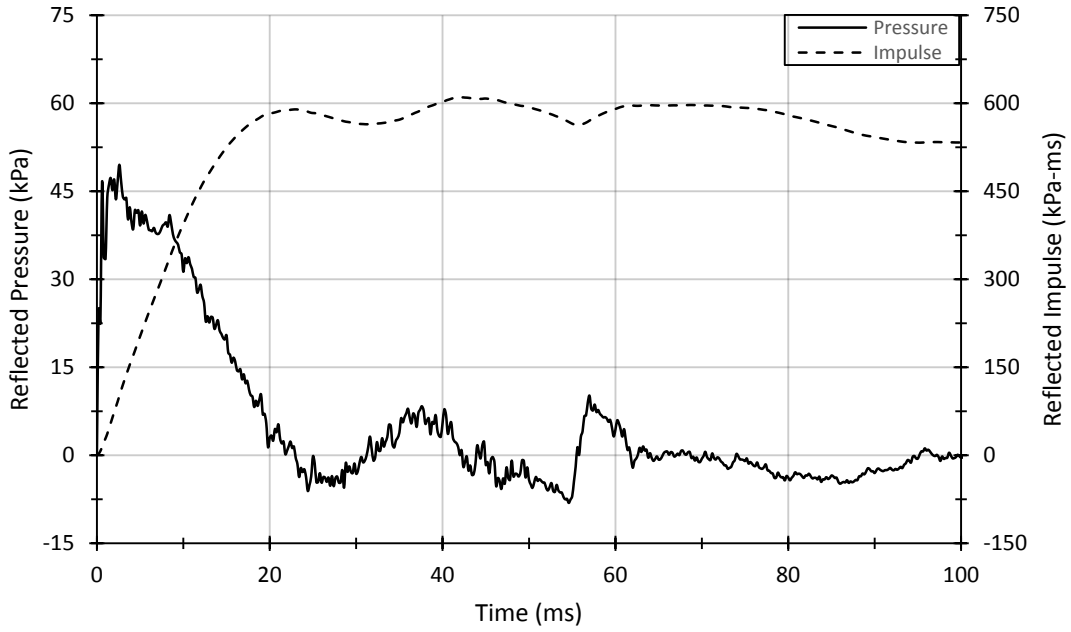

Figure 4.2: CLT 5-1 Pressure-Impulse Details

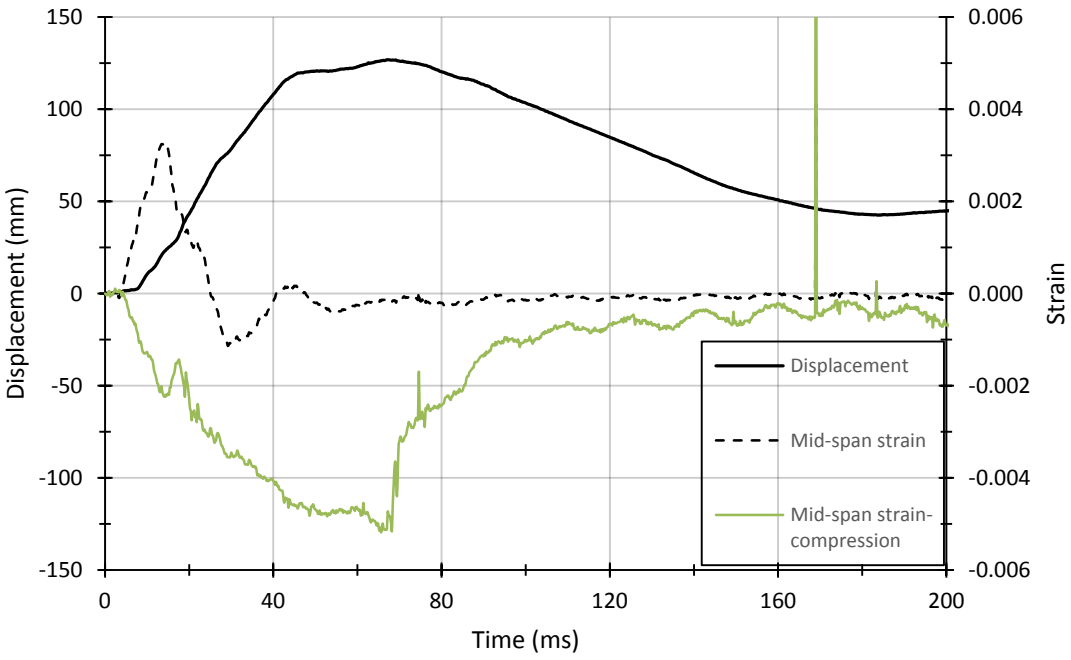

Figure 4.3: CLT 5-1 Strain and Displacement Details

Rotation at the bottom support and bending in the steel plate was observed. However, no significant yielding in the screws occurred. As rolling shear began to form at both ends of the slab, tension perpendicular to grain failure dominated the top joint. The failure occurred at the row of screws closest to the tension face. Some of the top connecting screws were fastened into end-grain, but the transverse layers did not seem to help reinforce the region and restrict the failure from occurring. Figure 4.4 and Figure 4.5 show the failure modes described above for both the top and bottom connections.

A) Tension Perpendicular to Grain Failure **B) Failure Plane**

Figure 4.4: CLT 5-1 Top Connection Failure Pictures

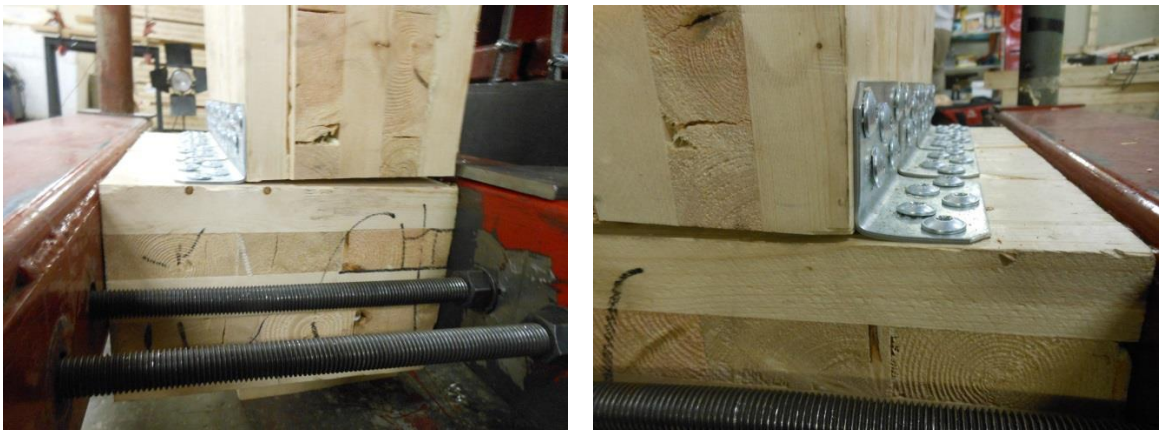

A) Rotation at Bottom Support **B) Close-Up of Steel Angles**

Figure 4.5: CLT 5-1 Bottom Connection Failure Pictures

4.2.2 CLT 5-2

The selected connection detailing for this test was chosen to improve the observed results for the typical connection details seen in test CLT 5-1. The top connection consisted of twelve Heco-Topix Zn Gelb A2L screws, with a diameter of 6 mm and a length of 300 mm, driven straight through the top supporting block into the end of the CLT slab. Additionally, five Zn Blau A2K screws with a diameter of 10 mm and a length of 120 mm. were installed into the tension face of the wall to act as reinforcement against splitting. The bottom connection was comprised of three ML24Z steel angles with three Heco-Topix Zn Blau screws per angle face. Figure 4.6 displays the top connection details for this test.

A) Top Reinforcement Screws

B) Top Connection Detail

Figure 4.6: CLT 5-2 Connection Details

Rotation at the bottom support was observed due to bending of the steel angles connecting the support block to the test specimen, with little to no yielding in the screws. As for the top connection, failure perpendicular to grain was also observed. However, the reinforcing screws shifted the surface of splitting towards the compression face. The splitting occurred at the tips of the reinforcing screws. Figure 4.7 and Figure 4.8 show the failure modes for both the top and bottom connections.

A) Overall Failure

B) Top Tension Perpendicular to Grain Failure

Figure 4.7: CLT 5-2 Top Connection Failure Pictures

A) Bottom Support Rotation

B) Close-Up of Bottom Steel Angles

Figure 4.8: CLT 5-2 Bottom Connection Failure Pictures

4.2.3 CLT 5-3

For this test, a similar top connection to that used in specimen CLT 5-2 was used, except that a total of twenty-seven 8 mm diameter and 300 mm length Heco-Topix Zn Gelb A2L screws were driven into the end of the test specimen. Additionally, five Zn Blau A2K screws with a diameter of 10 mm and a length of 120 mm were installed at the tension as well as the compression face to act as reinforcement against splitting. This connection detail was used at both slab ends. The joint was intentionally overdesigned by providing

an additional fifty percent in capacity based on the dynamic capacity approach in order to determine the behaviour of the connection when it is designed far beyond the blast standard requirements and to prevent failure in the connection. Figure 4.9 displays the connections for this test.

A) Tension Face **B) Bottom and Compression Face**

Figure 4.9: CLT 5-3 Connection Details

Tension perpendicular to grain was observed at the first row of vertical screws on the tension side, which coincided with the first transverse layer where rolling shear occurs and further weakened the slab. Figure 4.10 and Figure 4.11 show the failure modes described above for both the top and bottom connections.

Figure 4.10: CLT 5-3 Top Connection Failure Pictures

A) Left Side **B) Right Side**

Figure 4.11: CLT 5-3 Bottom Connection Failure Pictures

4.3 Angled Double-Threaded Screw Detailing

4.3.1 CLT 5-4

The top and bottom connections for this test were identical and consisted of another common connection type used in CLT construction for exterior wall to floor connection. Two double-threaded ZnA2K+DS-Beschichtet screws, measuring 8.5 mm in diameter and 350 mm in length, were installed at 60° from horizontal. In this test, the number of screws was selected based on the seismic design considerations described at the beginning of the chapter. It was ensured that the point where the screw thread changes was located at the interface between the slab and support block as shown in figure 4.12 A in order to pull the two wood pieces together. Figure 4.12 displays the top and bottom connections for this test.

A) Screw Installation Angle

B) Top and Bottom Connection

Figure 4.12: CLT 5-4 Connection Details

There was no observable damage to the CLT test specimen itself. However, the screws at the top and bottom connections all failed in combination of shear and withdrawal. This caused the slab to slide 23 cm until friction between the slab and blocks stopped the test specimen from moving any further. Figure 4.13 and Figure 4.14 show the failure modes.

A) Displacement Relative to Top Support

B) Failure of Top Connection Detailing

Figure 4.13: CLT 5-4 Top Connection Failure Pictures

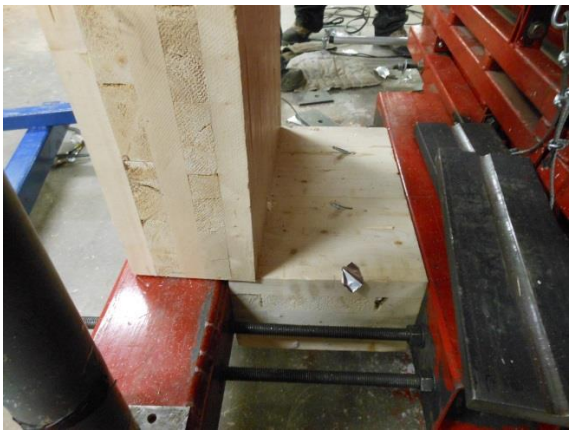

A) Displacement Relative to Bottom Support

B) Failure of Bottom Connection Detailing

Figure 4.14: CLT 5-4 Bottom Connection Failure Pictures

4.3.2 CLT 5-5

This test specimen is identical to CLT 5-4; however, eight double-threaded ZnA2K+DS-Beschichtet screws were used based on dynamic design following the blast design standard (2012). This was an attempt to increase the connection capacity beyond what was deemed adequate for the purpose of lateral in-plane design of the slab. Figure 4.15 displays the top and bottom connections for this test.

A) Top Connection

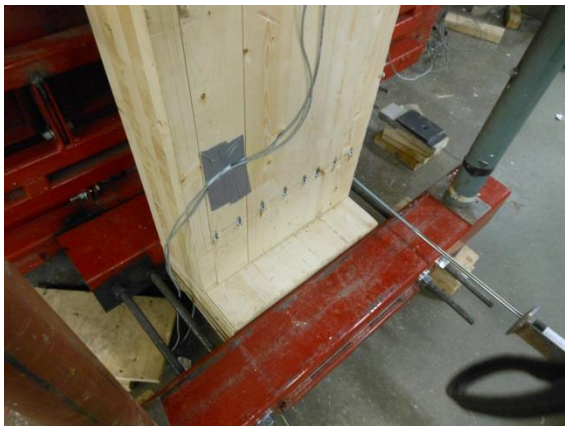

B) Bottom Connection

Figure 4.15: CLT 5-5 Connection Details

The increased connection capacity resulted in little sliding being observed. Significant rolling shear and tension perpendicular to grain failure was observed. Figure 4.16 and Figure 4.17 show the failure modes described above for both the top and bottom connections.

A) Perpendicular to Grain Failure

B) Close-Up of Top Failure Mode

Figure 4.16: CLT 5-5 Top Connection Failure Pictures

A) Left Side Rolling Shear

B) Right Side Rolling Shear

Figure 4.17: CLT 5-5 Bottom Connection Failure Pictures

4.4 Thin Angle Bracket Detailing

4.4.1 CLT 5-6

Due to wood's inherent poor tension perpendicular to grain capacity and its high compression capacity, the remainder of the tests performed in this experimental program were performed on bearing type connection details. This was done to limit and prevent the premature failure modes observed in the previous tests. In this test, the connection at both the top and bottom floors consisted of ML24Z thin steel angle brackets with Heco-Topix Zn Blau screws. Only two angle brackets were used and three screws per angle face. The capacity of this connection represented sufficient capacity per unit length of panel for seismic detailing. The connection was under-designed based on dynamic capacity considerations (70% reduced capacity compared to dynamic capacity of the panel), thus promoting failure in the connection. The purpose of this test was to achieve ductile damage in the connection without causing complete failure in the slab or connections. Figure 4.18 displays the top and bottom connections for this test.

A) Top Connection **B) Bottom Connection**

Figure 4.18: CLT 5-6 Connection Details

The slab deflected approximately 40 mm and had very little to no visible damage. All four angle brackets deformed significantly and in a similar manner. The screws remained embedded into the wood with little to no withdrawal failure observed. Figure 4.19 and Figure 4.20 show the failure modes for both the top and bottom connections.

A) Embedding of Top Steel Angles

B) Close-Up of Top Angles

Figure 4.19: CLT 5-6 Top Connection Failure Pictures

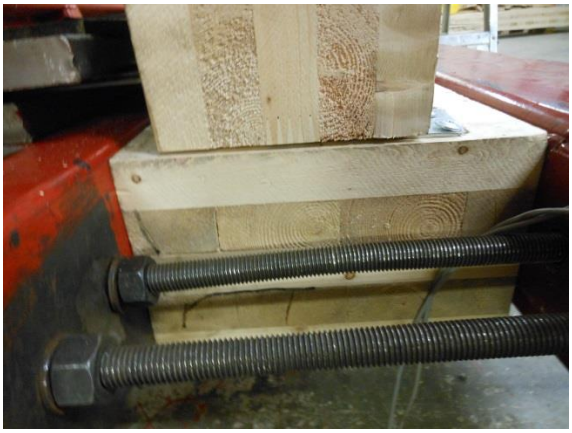

A) Displacement Relative to Bottom Support

B) Close-Up of Bottom Angle

Figure 4.20: CLT5-6 Bottom Connection Failure Pictures

4.4.2 CLT 5-7

Identical connection detailing to CLT 5-6 was used for this test but was subjected to approximately 15% higher reflected pressure and impulse.

The steel angles bent and crushed the tension face of the specimen. Some rolling shear was visible near the supports and finger joints in the specimen began to open up slightly

indicating initial signs of flexural failure. Figure 4.21 and Figure 4.22 show the failure modes for both the top and bottom connections.

A) Embedding of Top Steel Angles

B) Displacement Relative to Top Support

Figure 4.21: CLT 5- 7 Top Connection Failure Pictures

A) Rolling Shear at Bottom Support

B) Embedding of Bottom Steel Angles

Figure 4.22: CLT 5-7 Bottom Connection Failure Pictures

4.4.3 CLT 5-8

The connection detailing used for test CLT 5-8 was identical to tests CLT 5-6 and CLT 5-7 but shot with an additional 15% higher reflected pressure and impulse than test CLT 5-6. Similar behaviour was observed for this test as that described for tests 5-6 and 5-7. The angles at the top and bottom of the slab were bent and embedded into the slab, allowing

the slab to slide forward. Some bending as well as pullout of the screws connecting the angles to the blocks was observed. Figure 4.23 and Figure 4.24 show the failure modes.

A) Displacement Relative to Supports **B) Embedding of Top Angles**

Figure 4.23: CLT 5-8 Top Connection Failure Pictures

A) Embedding of Bottom Angles **B) Close-Up of Bottom Angles**

Figure 4.24: CLT 5-8 Bottom Connection Failure Pictures

4.4.4 CLT 5-9

This test was another reproduction of tests 5-6, 5-7 and 5-8 but tested at a slightly higher (5%) pressure-impulse combination than in test CLT 5-6. Increasing the pressure/impulse combinations for the four repeat tests presented was done to try and reach a level where flexural failure is achieved. Only damage to the slab was slight rolling shear near the

supports. Significant bending in the steel bracket and crushing in the wood tension face was observed. Additionally, some of the screw heads at the bottom support were pulled out. Figure 4.25 and Figure 4.26 show the failure modes the top and bottom connections.

A) Displacement Relative to Top Support

B) Embedding of Top Steel Angles

Figure 4.25: CLT 5-9 Top Connection Failure Pictures

A) Displacement Relative to Bottom Support

B) Embedding of Bottom Angle

Figure 4.26: CLT 5-9 Bottom Connection Failure Pictures

4.5 Stiff Angle Bracket Detailing

4.5.1 CLT 5-10

The connection detailing using thin steel angles (e.g. 5-6, 5-7, 5-8, and 5-9) resulted in a ductile behaviour of the angles themselves, absorbing the energy of the blast. Failure of the screws in those tests rarely occurred. Therefore, in order to investigate the possibility of attaining flexural failure in the CLT slabs, a 6.6 mm thick steel angle bracket was manufactured, and six Heco-Topix Zn Blau screws (8 mm diameter and 120 mm length) were used per angle face. The same connection detail was used for both the top and bottom end conditions. Figure 4.27 shows the connection detail.

A) Bottom Connection **B) Connection Close-Up**

Figure 4.27: CLT 5-10 Connection Details

No bending in the angles occurred, but screw deformation and wood crushing allowed for the ends of the slab to rotate without displacing. Rolling shear developed near the end supports. Flexural failure was initiated, as indicated by the spreading of the finger joints on the tension face of the slab, shown in Figure 4.28A. Figure 4.28 and Figure 4.29 show the failure modes described above for both the top and bottom connections.

A) Overall Failure

B) Top Rolling Shear

Figure 4.28: CLT 5-10 Top Connection Failure Pictures

A) Initial Flexural Failure

B) Bottom Rolling Shear

Figure 4.29: CLT 5-10 Bottom Connection Failure Pictures

4.5.2 CLT 5-11

The connection detailing for CLT 5-11 was identical to CLT5-10 but exposed to a higher pressure-impulse combination (approximately 17% higher pressure and impulse) in order to observe more damage. Similar to test specimen CLT 5-10, the angles remained intact while the screws deformed, allowing for the ends of the slab to rotate without displacing laterally. Rolling shear occurred at both ends of the slab, causing splitting failure. Flexure

failure was observed near the bottom third point with no significant damage in the connections. Figure 4.30 and Figure 4.31 show the failure modes.

A) Overall Failure

B) Top End Rotation

Figure 4.30: CLT 5-11 Top Connection Failure Pictures

A) Left Side Flexural Failure

B) Bottom End Rotation

Figure 4.31: CLT 5-11 Bottom Connection Failure Pictures

4.6 Balloon Construction Detailing

4.6.1 CLT 5-12

CLT 5-12 replicates boundary condition for balloon framing, where the walls extend pass the floor slab for multiple storeys. The support blocks were fastened to the tension face of the slab, and clamped to the shocktube end frame (by means of hand-tightening steel nuts on the connecting rods), as shown in Figure 4.32. Clamping the specimen is expected to provide some level of fixity that would be present in actual balloon construction. The symmetric end conditions of this test are representative of a middle storey wall segment. Figure 4.32 displays the top and bottom connections for this test.

A) Top Connection **B) Bottom Connection**

Figure 4.32: CLT 5-12 Connection Details

Although bending occurred in the middle of the slab, the applied pressure was not sufficient to cause complete flexural failure in the test specimen, as shown in Figure 4.33 A. Instead, rolling shear near the supports occurred. Very little damage occurred in the longitudinal laminates. Figure 4.33 and Figure 4.34 show the failure modes for both the top and bottom connections.

A) Tension Face

B) Right Side Rolling Shear

Figure 4.33: CLT 5-12 Top Connection Failure Pictures

A) Right Side Rolling Shear

B) Left Side Rolling Shear

Figure 4.34: CLT 5-12 Bottom Connection Failure Pictures

4.6.2 CLT 5-13

In an attempt to fail an undamaged specimen in flexure a 12% higher pressure and 4% higher impulse combination was employed in this test. The specimen experienced significant amounts of rolling shear. The magnitude of the applied load was sufficient to separate the finger joints, but the applied shot was not enough to cause a flexural failure through the entire cross-section. Figure 4.35 and Figure 4.36 show the failure modes for the top and bottom connections.

A) Left Side Flexural Failure

B) Right Side Flexural Failure

Figure 4.35: CLT 5-13 Top Connection Failure Pictures

A) Bottom Left Side Rolling Shear

B) Tension Face Flexural Failure

Figure 4.36: CLT 5-13 Bottom Connection Failure Pictures

Table 4.1: Test Results Summary

	Test	Driver Pressure (kPa)	Reflected Pressure (kPa)	Positive Impulse (kPa-ms)	Positive Phase Duration (ms)	Maximum Midspan Deflection (mm)	Failure Mode
End-Grain Screw Detailing	CLT 5-1	452.3	49.5	590.0	23.0	126.4	Connection in wood splitting
	CLT 5-2	481.3	60.9	683.1	23.4	221.5	Connection in wood splitting
	CLT 5-3	551.6	56.7	658.2	22.2	98.9	Connection in wood splitting
60° Double Threaded Screw Detailing	CLT 5-4	532.3	58.9	884.3	28.0	264.1	Screw tension
	CLT 5-5	531.6	56.1	646.0	23.0	74.9	Connection in wood splitting
Ductile Angle Detailing	CLT 5-6	482.6	54.1	628.4	23.2	65.1	Angle deformation
	CLT 5-7	517.8	62.4	721.1	23.8	78.3	Angle deformation
	CLT 5-8	561.9	62.1	717.6	24.0	74.7	Angle deformation
	CLT 5-9	572.3	56.8	670.9	22.0	90.0	Angle deformation
Stiff Angle Detailing	CLT 5-10	620.5	68.6	799.5	23.4	103.5	Initial flexural
	CLT 5-11	689.5	65.3	936.0	28.0	241.2	Flexural failure
Balloon Construction Detailing	CLT 5-12	552.3	52.8	696.7	23.2	59.3	Initial flexural
	CLT 5-13	595.0	59.2	722.8	23.0	76.6	Initial flexural

CHAPTER 5 - Discussion

5.1 General

This chapter discusses the behaviour of the CLT panels with various connection details tested during this experimental program. Emphasis is placed on the connection behaviour especially with regard absorbing energy through ductile failure or providing sufficient strength and stiffness to allow the CLT slabs to attain their ultimate capacity. The suitability of using simplified analysis techniques such as single-degree-of-freedom analysis is also discussed using dynamic analysis.

5.2 Dynamic Test Results

5.2.1 Behaviour of CLT Panels under Idealized Pin-Ended Conditions

As presented in Chapter 2, prior to the current study, an experimental program was initiated where five-ply CLT panels were tested in order to establish their behaviour under idealized pin-ended conditions (Poulin et al., 2017). This series of tests would serve as a reference to the measurements made in the current study since the material in both programs consisted of exactly the same CLT size and grade and was obtained from the same manufacturer.

The ultimate failure observed for the CLT slabs with pin-ended support was consistently characterized by flexure failure with the maximum deflection occurring at mid-span in the constant moment region. Figure 5.1 shows a typical failure observed in the simply supported tests. The ultimate failure occurred at an average reflected pressure and impulse of 54.8 kPa and 596.2 kPa-ms, respectively, (Poulin et al., 2017).

Figure 5.1: Typical Simply Supported Flexural Failure (Poulin et al., 2017)

Using these experiments as an average baseline for comparison with the current study's results, the effects of realistic boundary conditions on CLT panels subjected to blast loads is evaluated in the following sections.

5.2.2 Typical End-Grain Screw Detailing

The end grain connections used in specimens CLT 5-1 to CLT 5-3 was observed to cause premature failure in the CLT slab system at the connections. Instead of providing sufficient strength for the slab to reach its full flexural capacity, premature failure at the end of the wall panel caused the test specimens to fail in a different way than that assumed and observed for the idealized pin-ended conditions. For specimen CLT 5-1, stress concentrations formed at the tip of the connecting screws and splitting (i.e. tension perpendicular to grain) governed the failure at the row of screws closest to the tension side of the slab. Although this slab was shot at a similar pressure-impulse combination as the simply supported test specimens (P_R = 49.5 kPa, I_R = 590.0 kPa-ms), a completely different failure mode was observed. Although it is well-known that wood is weak in tension perpendicular to grain and that splitting failure should be avoided even when the structural element is subjected to static loading, such failure was not expected because the connection was designed to resist 20% more loads than the expected dynamic reaction. The observed behaviour is of great concern because it may lead to collapse of the

structure and loss of life. Although based on very limited data, such connection detailing is strongly cautioned against for blast design considerations.

Reinforcement of tension perpendicular to grain splitting has in recent years been researched and designed for using self-tapping screws installed in the perpendicular direction to the wood fiber and near the location of the end grain screws (e.g. Trautz and Koj, 2009). In an attempt to improve the behaviour observed in specimen CLT 5-1, screws were installed from the tension face to reinforce the joint. The number of screws in the end grain was reduced to further emphasize the positive effect of the reinforcing screws. Without the reinforcing screws, this connection would be under-designed according to the Canadian blast design standard (CSA 2012). The pressure and impulse were increased by 23% and 16%, respectively, compared to the shot specimen CLT 5-1 was subjected to. Although the connection was under-designed, the failure shifted towards the compression face, engaging more wood material and thereby increasing the splitting capacity. Figure 5.2 shows this shift in failure plane.

A) CLT 5-1 **B) CLT 5-2**

Figure 5.2: End-Grain Connection Failure Planes

Despite the improvement in behaviour, the brittle failure obtained in this test emphasizes the fact that end grain screw connections are not suitable for blast design. This is further emphasized in the test conducted on specimen CLT 5-3, where the number of screws was increased to resist 50% more load compared to test CLT 5-1. The pressure-impulse combination for specimen CLT 5-3 was comparable to that obtained for specimen CLT 5-2. Reinforcing on both the compression as well as the tension face of the slab was used.

It was not deemed economically feasible to enhance such connection type beyond that presented in specimen CLT 5-3. Despite such effort, splitting failure was observed. Figure 5.3 compares the displacement-histories for specimens CLT 5-1 to CLT 5-3 at the specimen mid-span.

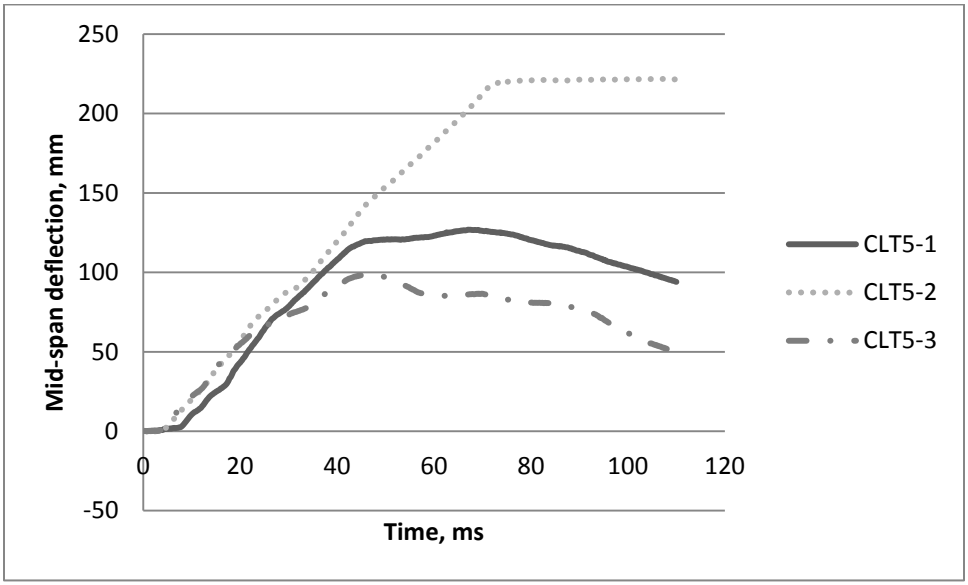

Figure 5.3: End-Grain Connection Mid-Span Displacements

As expected, the CLT 5-2 specimen experienced more deflection due to the reduced capacity (fewer end grain screws) intentionally selected for this specimen. When comparing specimens CLT 5-1 and CLT 5-3, a slight improvement on the deflection profile is observed for specimen CLT 5-3 due to the added number of screws and reinforcement, however, the added benefit cannot justify the increase number of screws and the time and cost associated with such installation.

Based on the findings discussed above, it can be concluded that providing reinforcing screws only slightly enhances the behaviour of the CLT slabs. It is therefore not advisable to employ such retrofit technique to existing CLT wall systems for platform type construction. In general, it can be noted that end grain connections are vulnerable to out of plane dynamic pressure waves, and should be avoided in new construction where a risk of blast is present.

5.2.3 Angled Double-Threaded Screw Detailing

Tension perpendicular to grain splitting and shear failure in connections were observed in this group of connectors. Seismic design detailing for specimen CLT 5-4 was found to be insufficient to resist the out-of-plane pressure applied. The screws at the top and bottom supports failed near the shear plane between the blocks and the test panel. The brittle failure observed at the connections is hazardous and can lead to potential collapse of the structure. Based on the results it can be concluded that angled screws even those with sufficient capacity to resist in-plane seismic loading would fail in a brittle manner and cause the entire CLT slab to become a projectile. This would completely eliminate the wall's ability to carry loads from floors above and also increase the risk on injuries of the building occupants.

Even when the number of screws was increased by four times in specimen CLT 5-5 compared to CLT 5-4 in order to meet the requirements for connection design following the Canadian blast design code (CSA 2012), brittle tension perpendicular to grain failure was still observed.

In general, it can be noted that typical gravity load resisting connection detailing, even though significantly enhanced and/or reinforced seem to perform poorly under shocktube induced dynamic loading.

5.2.4 Thin Angle Bracket Detailing

Observations made in the previous sections of this chapter highlight the deficiencies associated with using screws in the end grain of the CLT slab. In an attempt to improve on the behaviour, bearing type connections were investigated. This is in principle similar to bearing types successfully used by others in the context of light frame wood stud walls (Viau et al., 2016). The choice of bearing supports was meant to promote compression rather than tension perpendicular to grain failure and thin angles were meant to deform and provide energy dissipation in the system. In order to show consistency in behaviour, multiple tests were conducted with the only difference being in the pressure and impulse combinations to which the specimens were subjected. This also allowed to establish the limit to which the connection could be pushed without any catastrophic failure occurring.

In all tests involving the thin angle brackets (CLT5-6 to CLT 5-9), the steel bracket deformed significantly and crushed the wood on the tension face. No significant failure was observed in the CLT panel itself. Although this type of failure mode goes against the design philosophy outlined in the Canadian blast design standard (CSA 2012), where the connections are typically over-designed to allow the member to fully develop its capacity and ductility, for a material like wood, relying on the connection to yield is essential in enhancing the ductility and overall performance of the system. The difficulty is of course in finding the balance between yielding the connections to obtain adequate ductility while preventing complete failure which will compromise the performance of the building and the safety of the occupants. Ideally, the connections would provide the desired ductility ratio and not reach failure before the slab reaches its ultimate flexural failure. In order to investigate and optimize this concept further more research needs to be done on ductile type connections, where the yielding is isolated in connections with large enough deflection capacity to allow the wood member to fully develop its capacity.

Figure 5.4 shows a still picture from the video of specimen CLT 5-9 at maximum displacement where it can be seen the connections has translated significantly in the horizontal direction while no damage to the CLT specimen itself could be observed. This includes rolling shear failure which typically occurs at relatively low load levels. The majority of the energy was clearly observed in the connections.

An important point to mention is that although both the angle and the screws were under-designed based on the requirements in the blast design standard (CSA 2012), the overall performance of the wall slab was significantly improved due to the ductile failure.

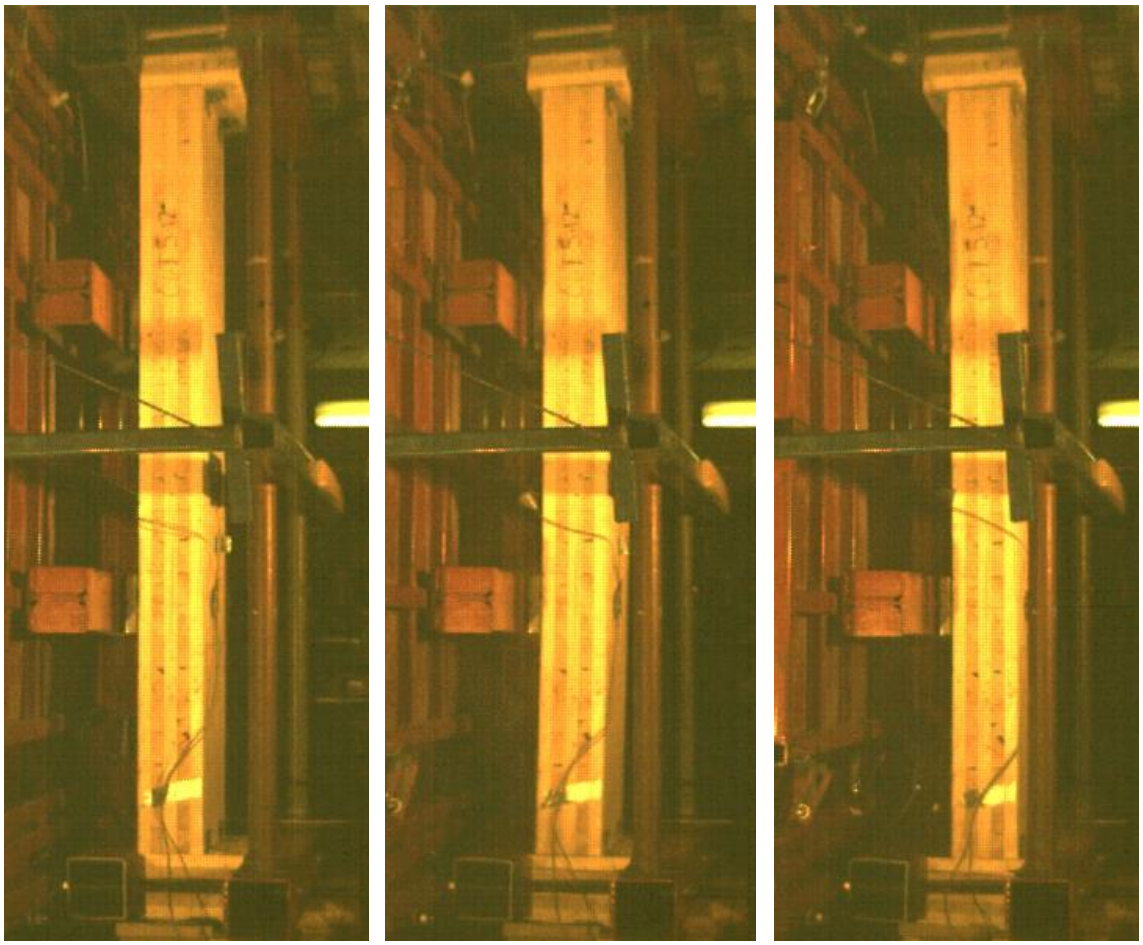

A) Initial Position B) Displaced Shape C) Maximum Displacement

Figure 5.4: CLT5-9 Displacement Progression (Max at 90 mm at 42ms)

The displacement-time history of the connection was measured for this specimen and subtracted from the total displacement profile measured at mid-span, as seen in Figure 5.5. The figure shows a comparison between the panel displacement for the case of idealized simply supported condition and that with connections. An example was used from Poulin (2017), where it fully recovers the measured displacement. The specimen from Poulin (2017) was exposed to a reflected pressure and impulse of approximately Pr = 55 kPa and Ir = 600 kPa-ms. Comparing the specimen tested in the current study with the one from Poulin (2017) in Figure 5.5 clearly shows that although the reflected pressure and impulse combination was approximately 16% higher in the CLT 5-8

specimen, significantly less displacement was observed in the CLT panel itself. This is attributed to the connection absorbing some of the energy imparted on the specimen. The CLT panel was exposed to much less energy as clearly demonstrated through the reduced deflection.

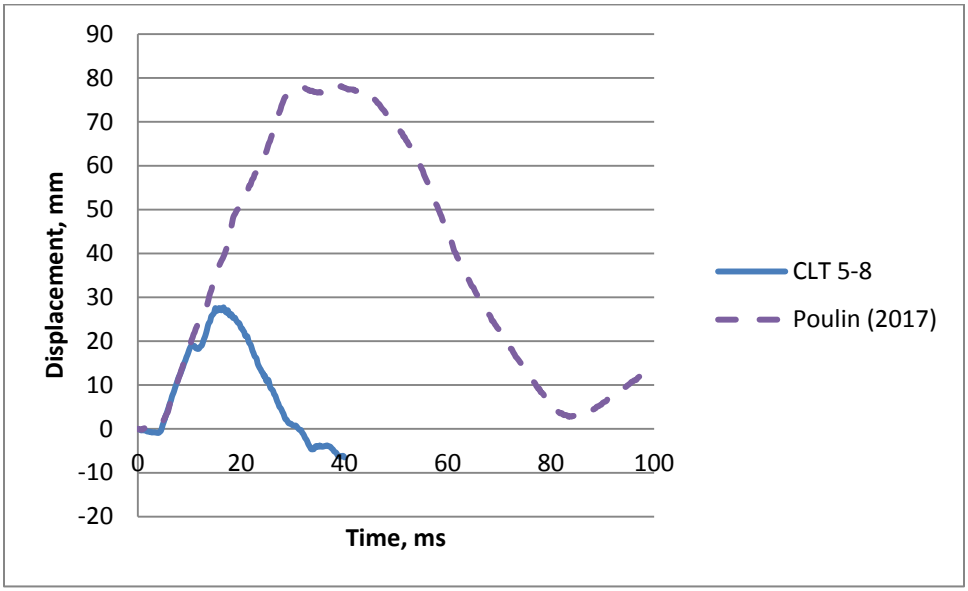

Figure 5.5: CLT 5-8 Bending Deflection vs. Previous Study Results

5.2.5 Stiff Angle Bracket Detailing

The previous section clearly demonstrated the concept of yielding the connections and thereby dissipating the energy without damaging the CLT panel. This may limit the system's stiffness and ultimate capacity because the panel may not reach its ultimate strength. A bearing type connection with sufficient capacity to meet the requirements in the blast design standard was investigated. Relatively thick steel angles were manufactured and used as boundary connections for the CLT slab in order to attain the ultimate failure in the slab while maintaining the integrity of the support connection. This approach could be considered as a viable alternative to that presented in the previous section (thin angles). Although favorable results were obtained for the case of thin steel angles, premature failure is possible if the ultimate displacement of the connectors is reached before the failure of the slab. The slab ends were assumed to freely rotate and that was thought to be an advantage from a modeling point of view since no lateral

translation and free rotation would mean that simply supported boundary conditions could be assumed. The validity of this assumption is investigated further in section 5.3.

The displacement-time history of the connection was also subtracted from the total displacement profile measured at mid-span. Figure 5.6 shows a comparison between the panel displacement for the case of idealized simply supported condition and that with connections. Although the pressure and impulses for the tests with heavy steel brackets were 22.1% and 45.6% higher than the average pressure and impulse for the case of simply supported end conditions respectively, same or lower displacement was recorded for the specimen with connection.

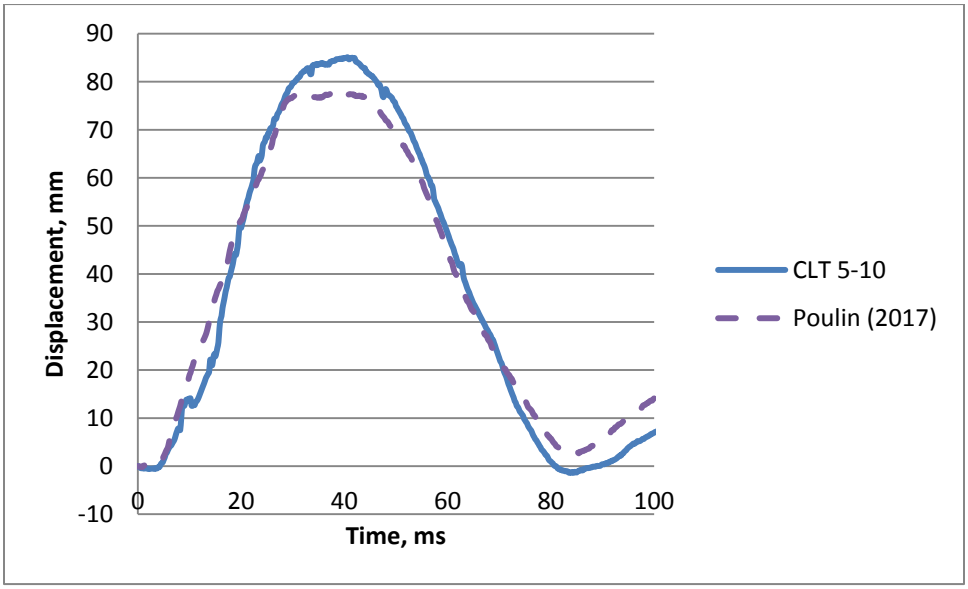

Figure 5.6: CLT 5-8 Bending Deflection vs. Previous Study Results

Significantly less damage to the CLT slabs with connections was observed, as can be seen in Figure 5.7, which is a still shot taken from the video recording at maximum displacement. This can again be attributed to the connection absorbing some of the energy imparted on the specimen.

As was observed in the video recording (and to a lesser degree in Figure 5.6), the connection translated significantly (max 17.9 mm) due to the slip between the screws and the wooden blocks. The screw connection with the stiff steel angle also provided some rotational restraint as demonstrated in Figure 5.7 through the small amount of separation

between the slab and the block simulating floors. As will be shown in Section 5.3 this will have some implication on the modeling aspect of the CLT wall system.

Figure 5.7: CLT5-10 at Maximum Displacement (85 mm at 41ms)

5.2.6 Balloon Construction Detailing

This connection detailing puts emphasis on two important concepts learned from the previous tests, namely, providing bearing support and end restraint due to the floor diaphragm action. Since there was no possibility to fail the connections, the level of pressure and impulse combinations that would cause failure in the CLT slab was of interest. For test specimen CLT 5-12, although pressure and impulse combination similar to the case causing complete failure in the simply supported end conditions was applied on this specimen compared, only superficial damage was observed in the CLT specimen.

This is attributed to the restraint that the boundary joints provided. The slabs with balloon construction detailing completely recovered their displacements and return back to their original position with only minor damage. The slab can be assumed to have significant axial capacity remaining to prevent building collapse. Figure 5.8 shows the deflected shape of the slab with emphasis on the deformation at the connection. It can be seen that a near fixed boundary conditions is observed at maximum deflection.

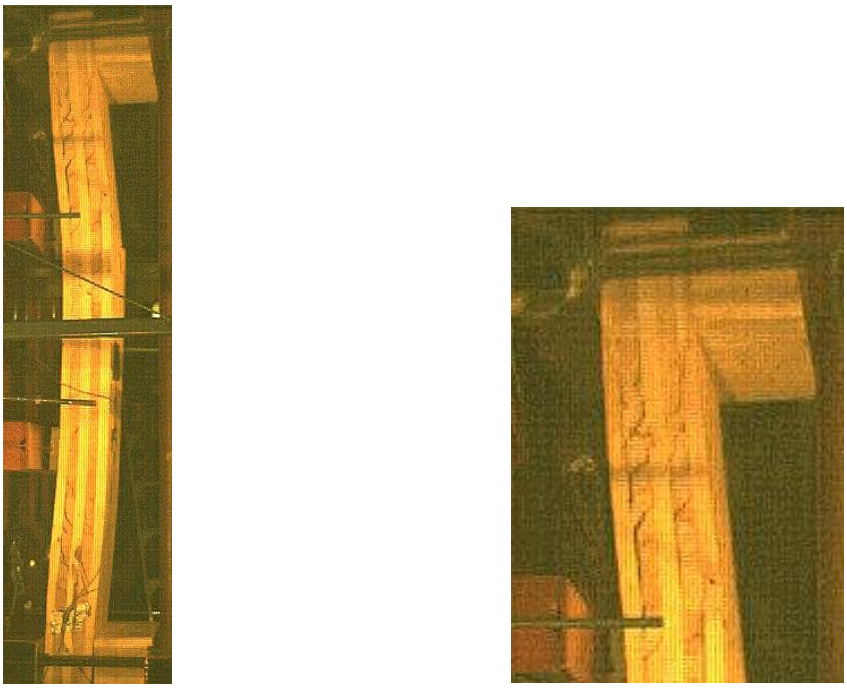

A) Overall Failure **B) Support Fixity**

Figure 5.8: CLT5-12 at Maximum Displacement (90 mm at 42ms)

5.3 Investigating the Suitability of Simplified Models

As described in Chapter 2, a material predictive model was developed for CLT slabs with simply supported boundary conditions (Poulin et al., 2017). Regardless of what connection is used, timber is generally assumed by designers to have simply-supported end conditions because the tension perpendicular to grain capacity is typically insignificant to develop moment resistance at the connection. This section aims at investigating the suitability simple model with simply supported assumptions for timber (specifically CLT) members. Some of the test configurations failed prematurely in splitting such as the ones with screws in end grain (list the specimens). Although

designers may still assume that such connections can be idealized as simply supported, the test results clearly show that a model developed for the behaviour of the CLT slab and that assumes simply supported end conditions would not be suitable to model such configuration.

The modeling was done in RC Blast (Jacques, 2014), which is a freely available software used to conduct single degree of freedom analysis. Using the material-predictive model developed by Poulin et al. (2017), the software was used to predict the deformation-time response of the CLT slabs while using the actual pressure-time histories generated during the tests. Investigating more complex models was deemed outside the scope of the current research.

5.3.1 SDOF Model Inputs

Several inputs are required for SDOF models to provide an accurate prediction of the behaviour of the test specimen such as structural properties of the slab as well as loading information. The loaded area was that of the load transfer device and was measured to be 3.55 m^2. The mass of the system is comprised of the mass of the test specimen in addition to the mass of the load transfer device (286.32kg and 91.3kg respectively). The actual pressure-time history from the test was used. The resistance curve was obtained from Poulin et.al. (2017) and adjusted for the span of slab. The dimension, grade and loading mechanism were all the same as those used in Poulin et al. (2017). The following resistance curve and $K_{L/M}$ values for simply supported five-ply CLT panels may be used in the model.

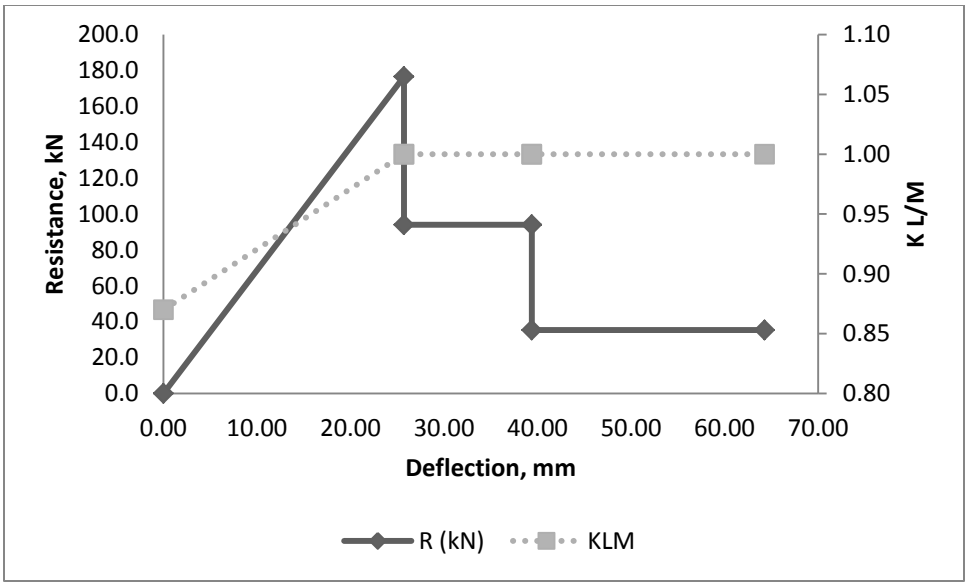

Figure 5.9: Five-ply CLT Resistance Curve for L = 2082.8 mm

5.3.2 Model Results

As mentioned earlier, not all connection types are suitable for the comparison with the simplified analysis since it can be confirmed through observation of the failure mode that the shape function for simply supported condition is not applicable. This includes the end-grain screw connections and angled double-threaded screws, which resulted in tension perpendicular to grain failure at the connection. Another group of connections for which the SDOF model considered here would be inaccurate is the one with thin angles. The energy absorbed by the brackets needs to be included in the model. This could be done by conducting a multi-degree-of-freedom model or by using higher fidelity models such as finite element.

For any designer not privy to the presented results of deflection and failure modes the CLT slabs with stiff angle might be considered as simply supported. Figure 5.10 shows that SDOF models based on simply supported boundary conditions over-predicts the deflection by 30% at the time of peak deflection in the experimental data. Clearly, even for such simple case the SDOF model is not suitable in predicting the displacement-time history. The inability of the model to predict the behaviour is known only because of the video as the observations where unexpected and displacements of significant magnitude were observed.

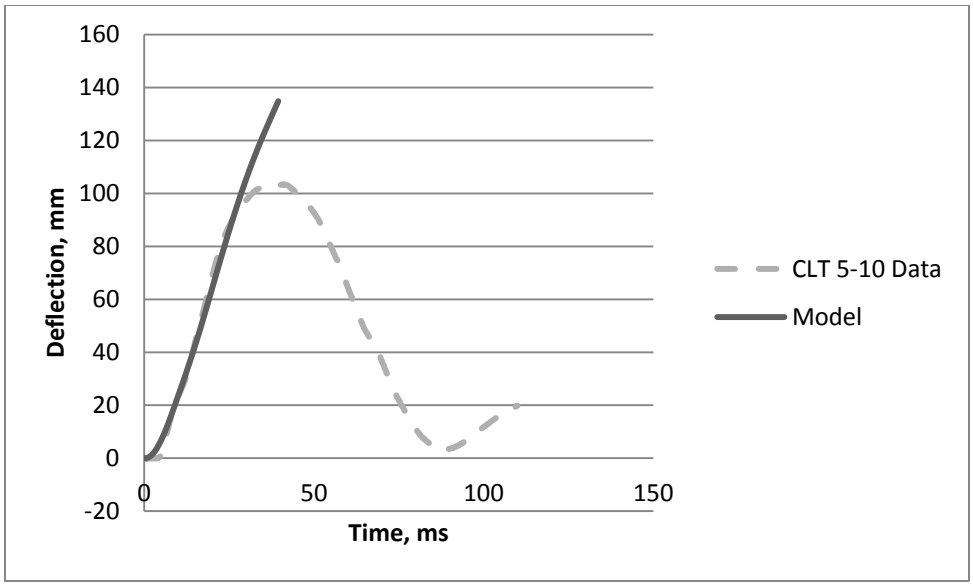

Figure 5.10: CLT 5-10 Model Prediction

CHAPTER 6 - Conclusion and Future Recommendations

6.1 General

The current study qualitatively assessed the behaviour of cross-laminated timber panels with realistic boundary conditions when subjected to blast loads. A total of thirteen tests were performed using the University of Ottawa shocktube on five-ply CLT panels using various end conditions. An emphasis was placed on damage levels and failure modes in comparison to previous CLT tests with idealized simply-supported conditions. The following sections summarize the key findings of this study and suggest possible future research.

6.2 Conclusions

Based on the findings in the current study, the following conclusions can be presented:

- Different failure modes were observed for each connection detail used, which did not coincide with the observed results of previous CLT tests with idealized pin-ended conditions.
- Typical connection with screws in end grain failed prematurely in tension perpendicular to grain at the connection location. The addition of reinforcing screws did not mitigate the brittle tension to grain failure.
- Connection details consisting of double-threaded screws inserted at sixty degrees from horizontal perform poorly when subjected to out of plane loading. Such failure is unfavorable in a blast event since it could lead to the wall becoming a projectile and also to a possible progressive collapse of the building.
- Although under-designed, thin steel angles provided significant energy dissipation through steel yielding and wood crushing. This resulted in reduced panel deflection and damage.
- Thicker steel angles still provided some energy dissipation through yielding in the screws as well rotational restraint of the slab ends.
- Tests on balloon construction assemblies exhibited significant rotational restraint of the slab end.

- Connection design based on capacity alone may not be sufficient. Additional considerations such as connection type and details should also be introduced in design to ensure adequate design reliability.
- Simplified models developed for idealized simply-supported conditions were found not to be adequate to describe the behaviour of the system. More advanced modeling techniques including multi-degree-of-freedom models or FEA may be required to adequately describe the behaviour when realistic boundary conditions are used.

6.3 Recommendations for Future Work

Based on the observations and results of the current study, several areas of research have been identified as requiring future work. These include the following:

- Static component testing for the different connection types should be performed to develop accurate predictive models for CLT panels with realistic boundary conditions.
- The effects of axial loads on the performance of CLT walls should be considered and incorporated into predictive models.
- Lacking from the current research project was the ability to measure the reactions. Since no reliable modeling technique exists that incorporates the effects of the connection relying on the applied pressure and impulse to evaluate the behaviour, proper analysis was no feasible. Future work should incorporate a method to evaluate or measure the reaction forces.
- Future work is suggested to further investigate and improve upon bearing connection types with ductile behaviour.

REFERENCES

Barrett, J., & Lau, W. (1994). *Canadian lumber properties*. Ottawa: Canadian Wood Council.

Biggs, J. M. (1964). *Introduction to structural dynamics*. New York,: McGraw-Hill.

Bogosian, D., & Avanessian, H. D. (2004). Blunt Trauma from Blast-Induced Building Debris. 31st Explosives Safety Seminar. San Antonio, TX.

Canadian Wood Council. (2010). Wood Design Manual. Ottawa, Ontario, Canada: Canadian Wood Council.

Ceccotti, A., Follesa, M., Lauriola, M. P., Minowa, C., Sandhaas, C., and Yasumura, M. (2006). "SOFIE Project: Test results on the lateral resistance of cross-laminated wooden panels." *First European Conference on Earthquake Engineering and Seismicity*,Geneva, Switzerland, 1-10.

Pei, S., Rammer, D., Popovski, M., Williamson, T., Line, P., & W. van de Lindt, J. (2016). An Overview of CLT Research and Implementation in North America. *World Conference on Timber Engineering*. Vienna, Austria, 7.

CSA. (2012). *CSA S850 - Design and assessment of buildings subjected to blast loads*. Mississauga: Canadian Standards Association Group, 5- 73.

CSA. (2014). *CSA O86 - Engineering design in wood*. Mississauga: Canadian Standards Association.

Dusenberry, D. (2010). *Handbook for blast-resistant design of buildings*. Hoboken, NJ: J. Wiley, 23-162.

FEMA.gov|Federal Emergency Management Agency. (2017). Retrieved September 17, 2017, from Federal Emergency Management Agency: www.fema.gov

FPInnovations. (2011). *CLT handbook: cross-laminated timber*. Québec: FPInnovations, 6.

Government of BC. (2009). *Bill 9 - Wood First Act*. Retrieved from Legislative Session: 1st Session, 39th Parliament: https://www.leg.bc.ca/39th1st/1st_read/gov09-1.html.

Government of Ontario. (2014). *Ontario Building Code*. Retrieved from CodeNews Issue 232 - Amendments to Ontario's Building Code Allowing Mid-Rise Wood Frame Buildings: http://www.mah.gov.on.ca/Page10816.aspx.

Jacques, E. (2014). *RCBLAST* (Version. 0.5.1) [Computer program]

Jacques, E., Lloyd, A., Braimah, A., Saatcioglu, M., Doudak, G., & Abdelalim, O. (2013). *Influence of high strain-rates on the dynamic flexural material properties of spruce-pine-fir wood studs*. Canadian Journal of Civil Engineering, 9.

Jansson, B. (1992). *Impact Loading of Timber Beams*. Vancouver, BC: University of British Columbia.

Krauthammer, T. (2008). *Modern Protective Structures*. Boca Raton, FL: CRC Press, 328.

Lacroix, D. (2013). *Behaviour of light-frame wood stud walls subjected to blast loading*. Ottawa: University of Ottawa.

Lacroix, D., & Doudak, G. (2013). *Modelling the Behaviour of Light-Frame Wood Stud Walls Subjected to Blast Loading*. 3rd Specialty Conference on Material Engineering & Applied Mechanics (pp. 1-10). Montreal, QC: CSCE.

Lacroix, D., & Doudak, G. (2014). *Investigation of Dynamic Increase Factors in Light-Frame Wood Stud Walls Subjected to Out-of-Plane Blast Loading*. Journal of Structural Engineering, ASCE, 1-10.

Lacroix, D., Doudak, G., & El-Domiaty, K. (2013). *Retrofit Options for Light-Frame Wood Stud Walls Subjected to Blast Loading*. Journal of Structural Engineering, ASCE, 1-8.

Liska, J. (1950). *Effect of Rapid Loading on the Compressive and Flexural Strength of Wood*. Madison, WI: United States Department of Agriculture.

Li, Y., and Lam, F. (2016). "Low cycle fatigue tests and damage accumulation models on the rolling shear strength of cross-laminated timber." *Journal of Wood Science*, 62(3), 251-262.

Lloyd, A., & Jacques, E. (2011). *Innovative and Cost Effective Blast Strengthening of Wood Framed Structures*. Ottawa, ON: University of Ottawa.

McCutcheon, W. (1977). *Method for predicting the stiffness of wood-joist floor systems with partial composite action*. Madison, WI: US Department of Agriculture.

Nadeau, J., & Bennett, R. (1982). *An explanation for the rate-of-loading and duration-of-load effects in wood in terms of fracture mechanics*. Journal of Materials Science, 2831-2840.

Polensek, A., & Schimel, B. (1986). *Rotational restraint of wood-stud wall supports*. Journal of Structural Engineering, 1247-1262.

Popovski, M., and Gavric, I. (2016). "Performance of a 2-Story CLT House Subjected to Lateral Loads." *Journal of Structural Engineering*, 142(4), E4015006.

Poulin, M., Viau, C., Lacroix, D., & Doudak, G. (2017). Experimental and Analytical Investigation of Cross-Laminated Timber Panels Subjected to Out-of-Plane Blast Loads. *Journal of Structural Engineering*.

NRC. (2015). *National Building Code of Canada*. Ottawa: National Research Council of Canada.

Sikora, K. S., McPolin, D. O., and Harte, A. M. (2016). "Effects of the thickness of cross laminated timber (CLT) panels made from Irish Sitka spruce on mechanical performance in bending and shear." *Construction and Building Materials*, 116, 141-150.

Sorensen, A., & McGill, W. (2011). *What to look for in the aftermath of an explosion? A review of blast scene damage observables*. Engineering Failure Analysis, 836-846.

Steiger, R., and Gülzow, A. (2009). "Validity of bending tests on strip-shaped specimens to derive bending strength and stiffness properties of cross-laminated solid timber (CLT)." International Council for Research and Innovation in Building and Construction, Duebendorf, Switzerland.

Sukontasukkul, P., Lam, F., & Mindess, S. (2000). *Fracture of parallel strand lumber (PSL) under impact loading*. Materials and Structures, 445-449.

Syron, W. (2010). *Strain rate-dependent behaviour of laminated strand lumber*. Orono, Maine: University of Maine.

Trautz, M., & Koj, C. (2009). *Self-tapping screws as reinforcement for timber structures.* Aachen, Germany: International Association for Shell and Spatial Structures.

U.S.A.C.E PDC. (2008a). *Methodology Manual for the Single-Degree-of-Freedom Blast Effects Design Spreadsheets (SBEDS)*: U.S. Army Corps of Engineers Protective Design Center Technical Report, 4-70, 9-1.

USADD. (2008). *Unified Facilities Criteria (UFC) 03-340-02 - Structures to Resist the Effects of Accidental Explosions*. Washington, D.C: United States of America Department of Defense.

USAF. (2006). *Vehicle Bomb Mitigation Guide*. Lackland AFB, Texas: United States Air Force.

Viau, C., & Doudak, G. (2016). Investigating the Behaviour of Light-Frame Wood Stud Walls Subjected to Severe Blast Loading. *American Society of Civil Engineers*.

Viau, C., & Doudak, G. (2016). Investigating the behaviour of typical and designed wall-to-floor connections in light-frame wood stud wall structures subjected to blast loading. *NRC Reseach Press*.

Yasumura, M., Kobayashi, K., Okabe, M., Miyake, T., and Matsumoto, K. (2016). "Full-Scale Tests and Numerical Analysis of Low-Rise CLT Structures under Lateral Loading." *Journal of Structural Engineering*, 142(4), E4015007.

Zhou, Q., Gong, M., Chui, Y. H., and Mohammad, M. (2014). "Measurement of rolling shear modulus and strength of cross laminated timber fabricated with black spruce." *Construction and Building Materials*, 64, 379-386.

APPENDIX A – Dynamic Test Results

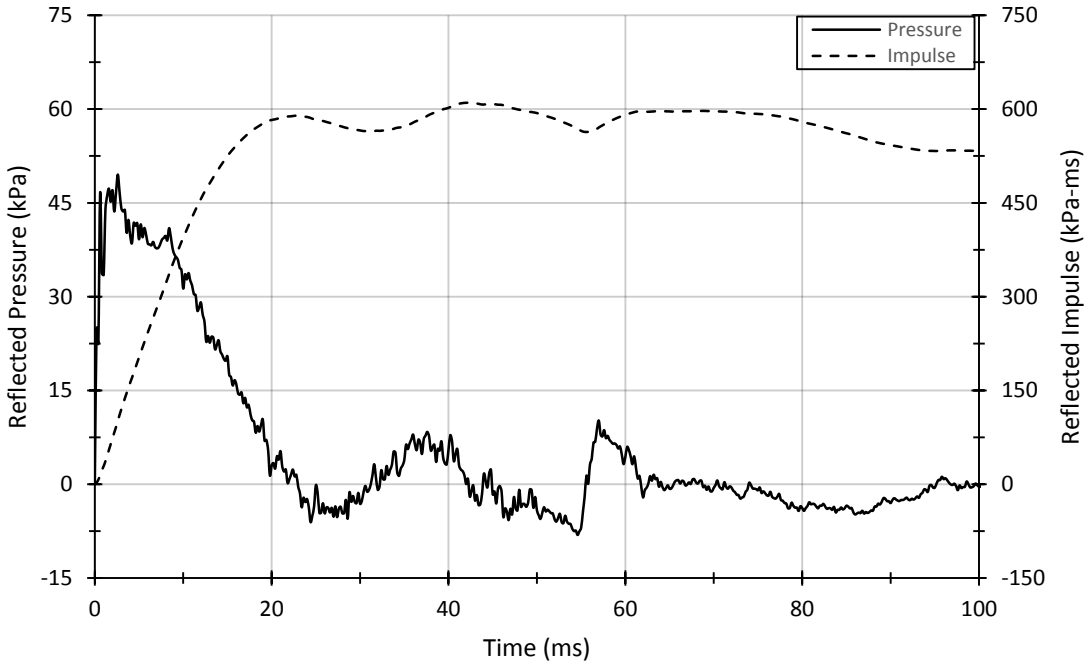

Figure A1.1: CLT 5-1 Pressure-Impulse Details

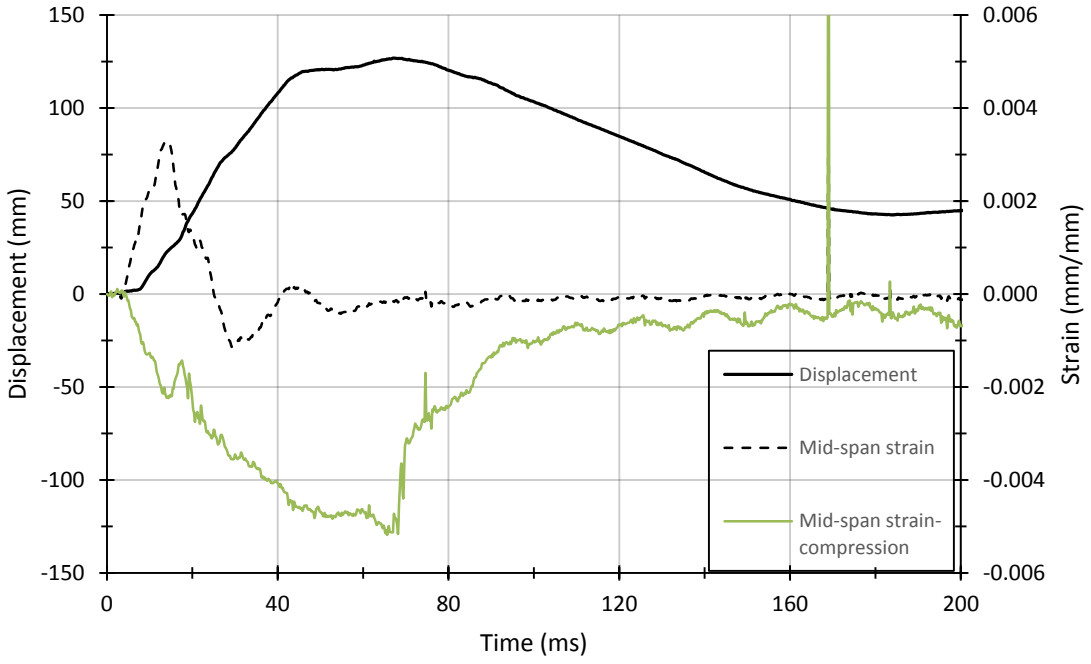

Figure A1.2: CLT 5-1 Strain and Displacement Details

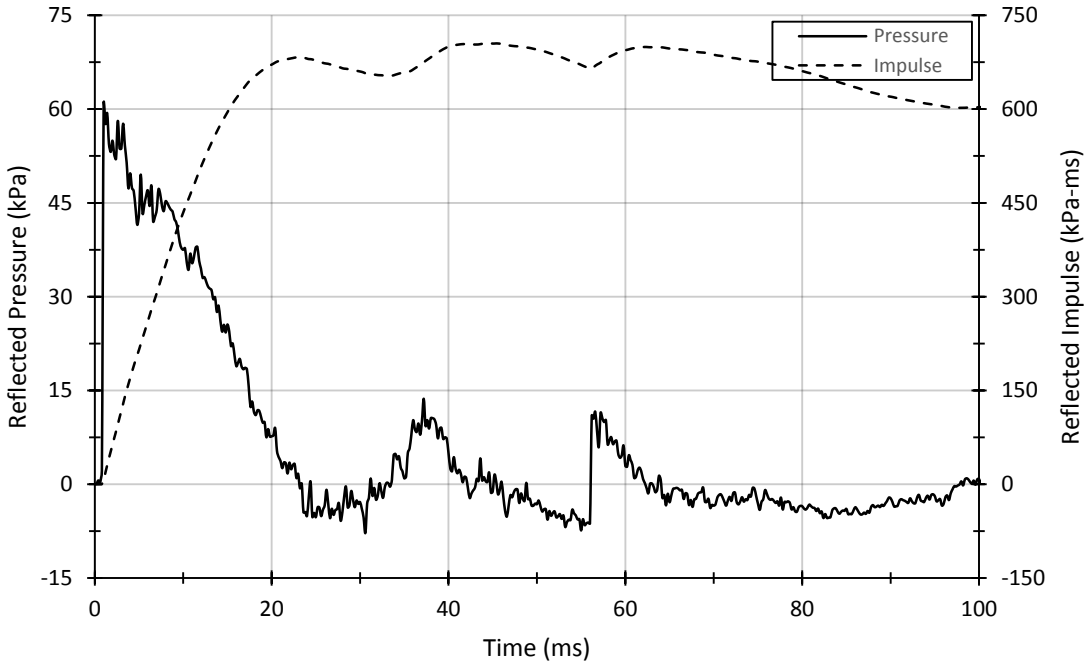

Figure A2.1: CLT 5-2 Pressure-Impulse Details

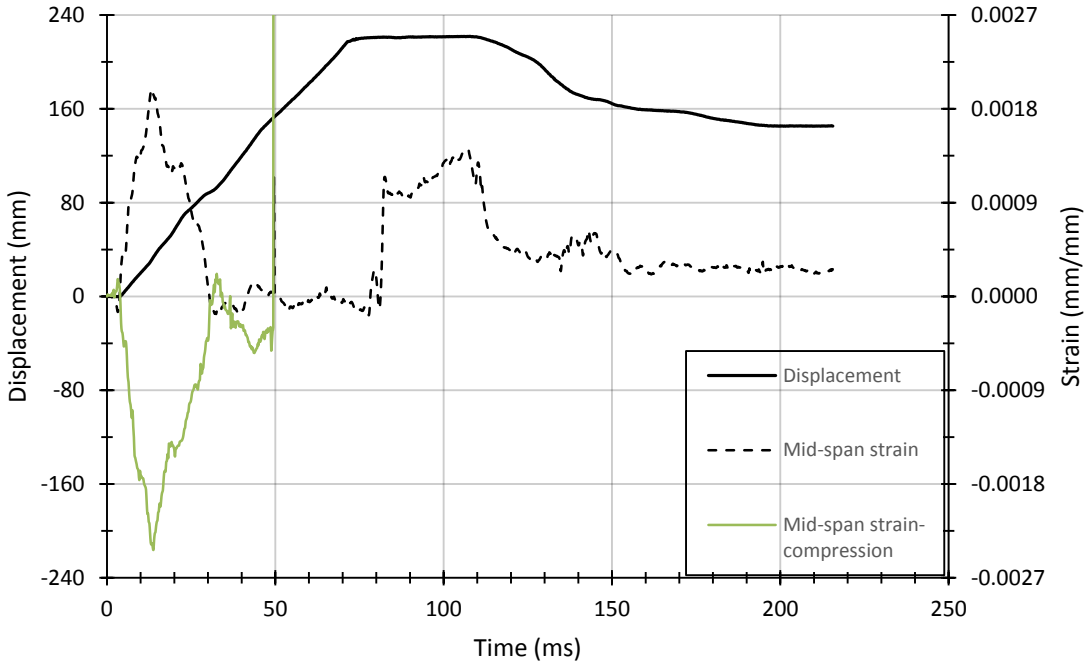

Figure A2.2: CLT 5-2 Strain and Displacement Details

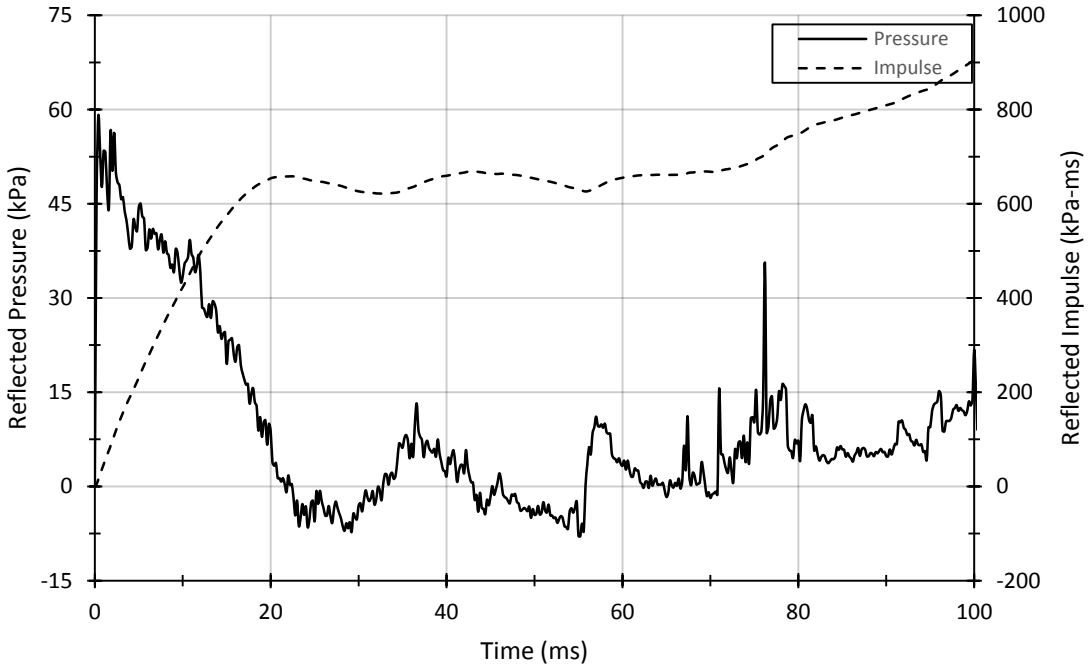

Figure A3.1: CLT 5-3 Pressure-Impulse Details

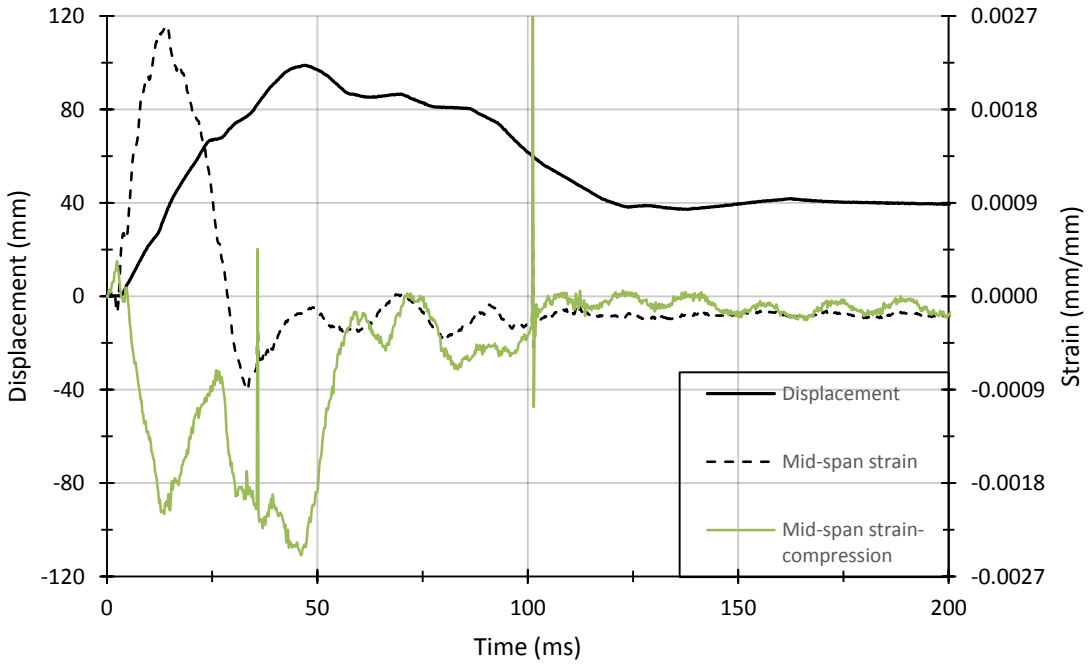

Figure A3.2: CLT 5-3 Strain and Displacement Details

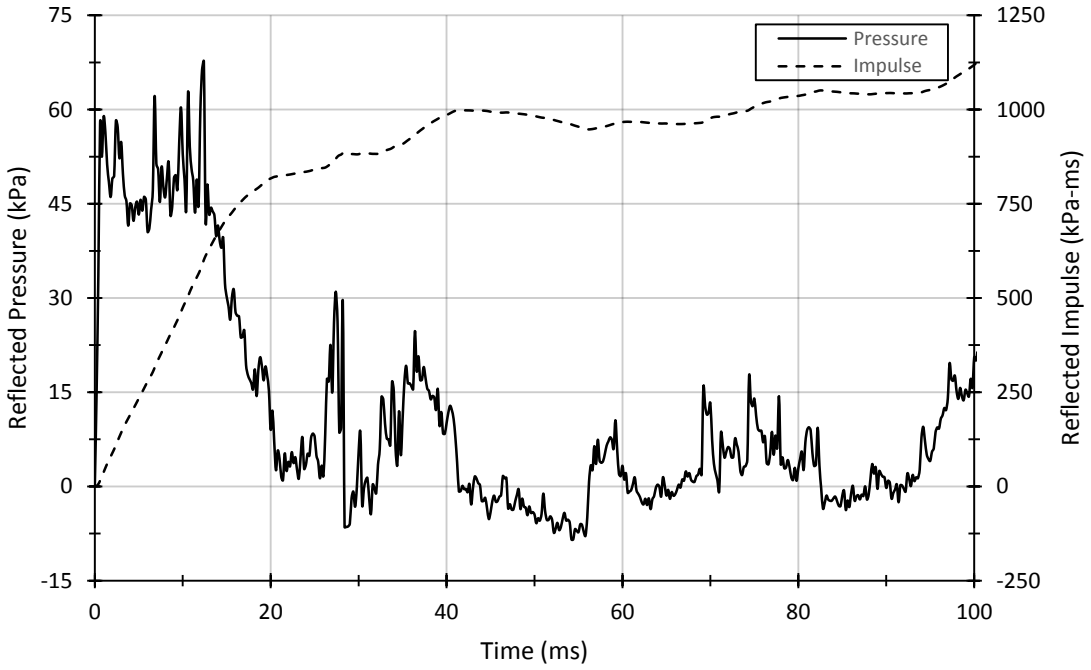

Figure A4.1: CLT 5-4 Pressure-Impulse Details

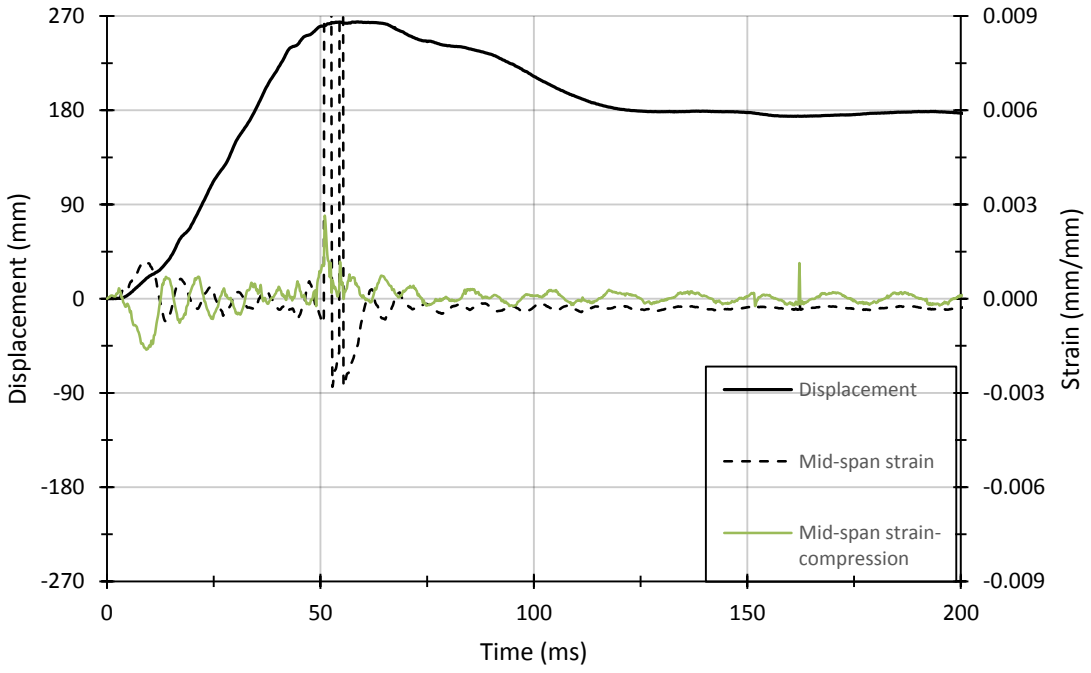

Figure A4.2: CLT 5-4 Strain and Displacement Details

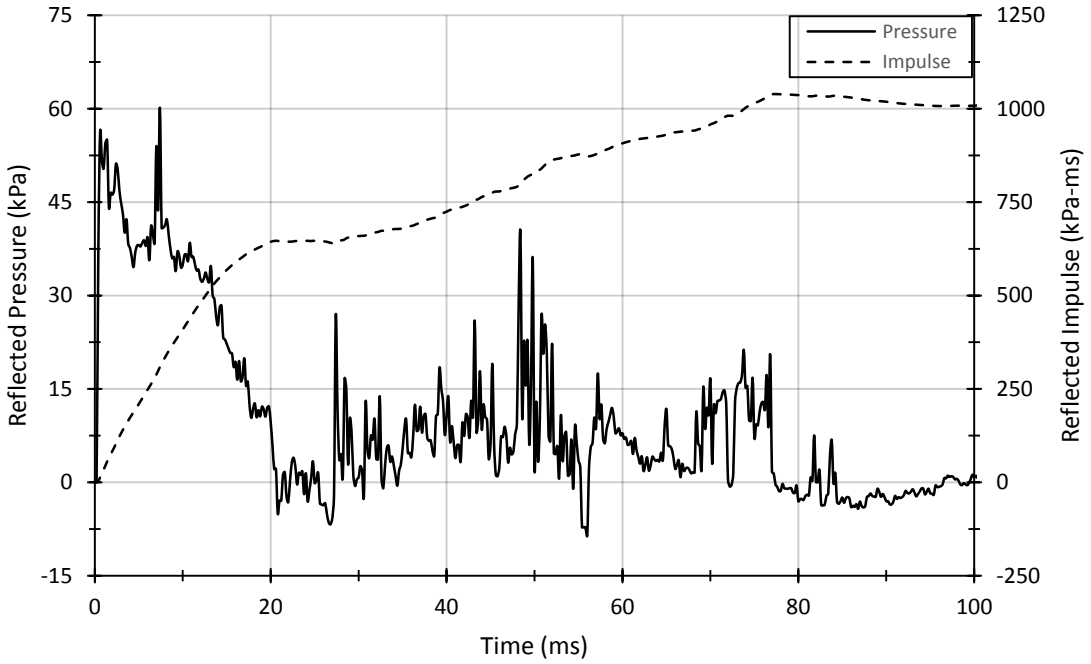

Figure A5.1: CLT 5-5 Pressure-Impulse Details

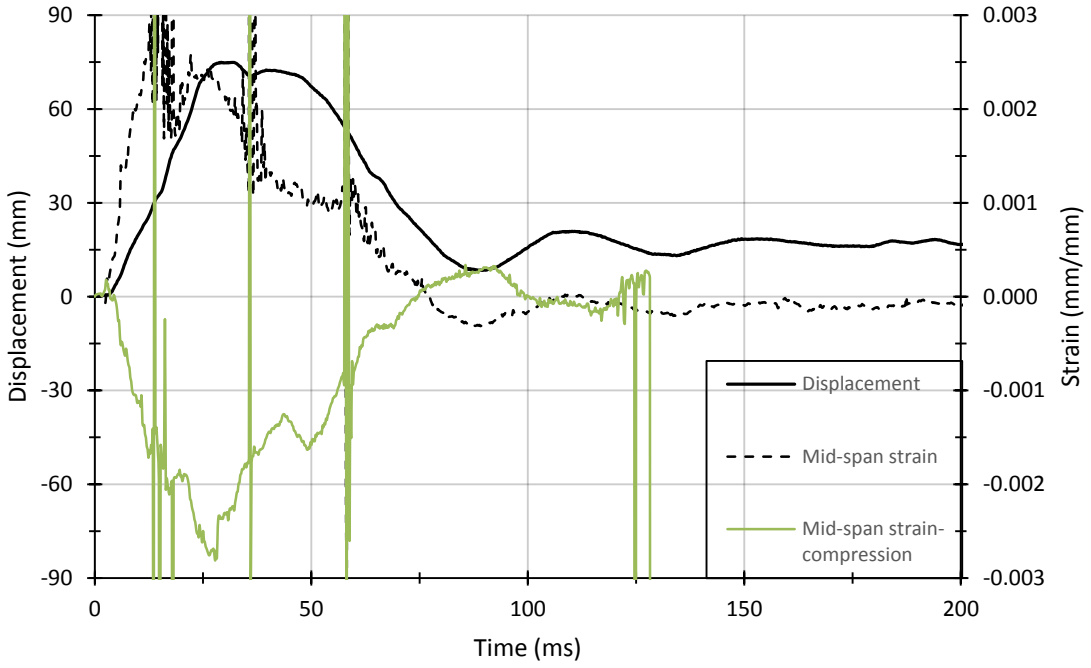

Figure A5.2: CLT 5-5 Strain and Displacement Details

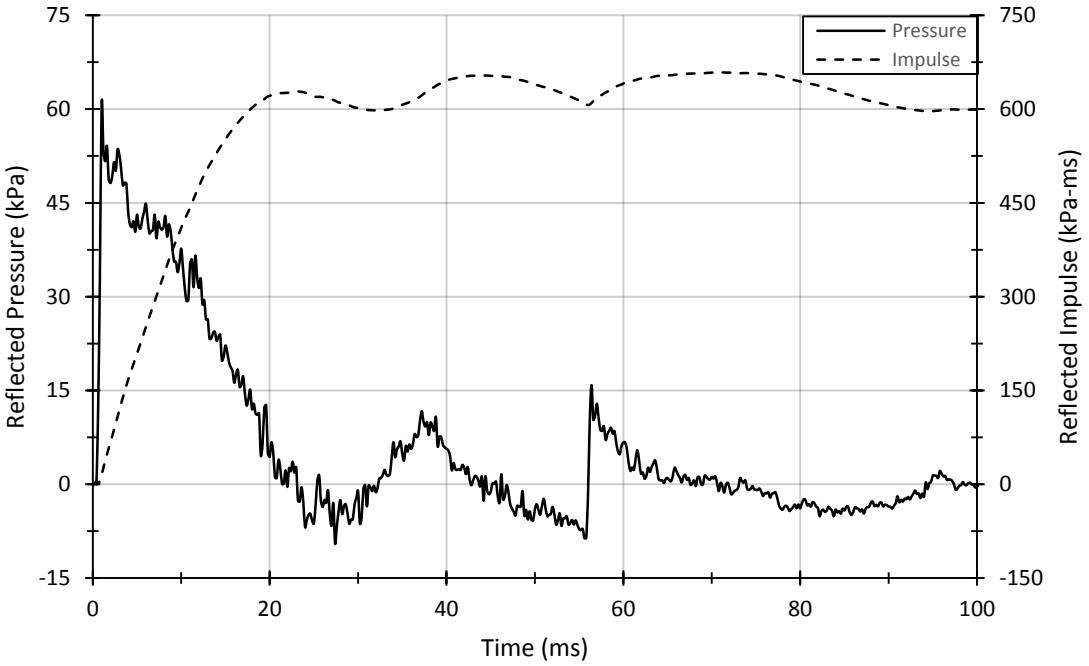

Figure A6.1: CLT 5-6 Pressure-Impulse Details

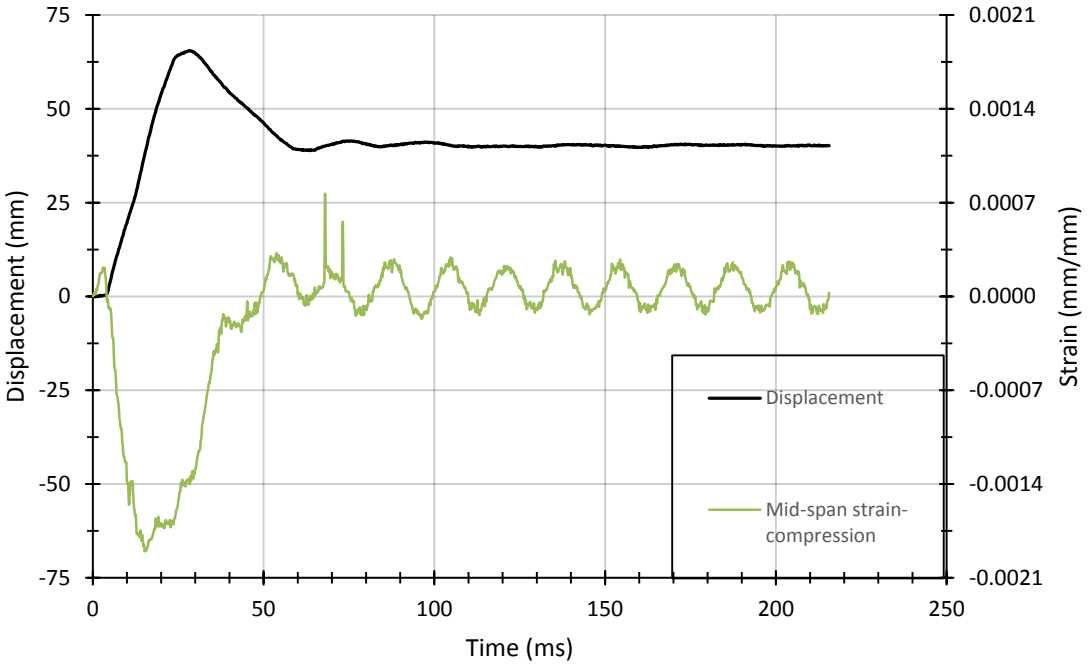

Figure A6.2: CLT 5-6 Strain and Displacement Details

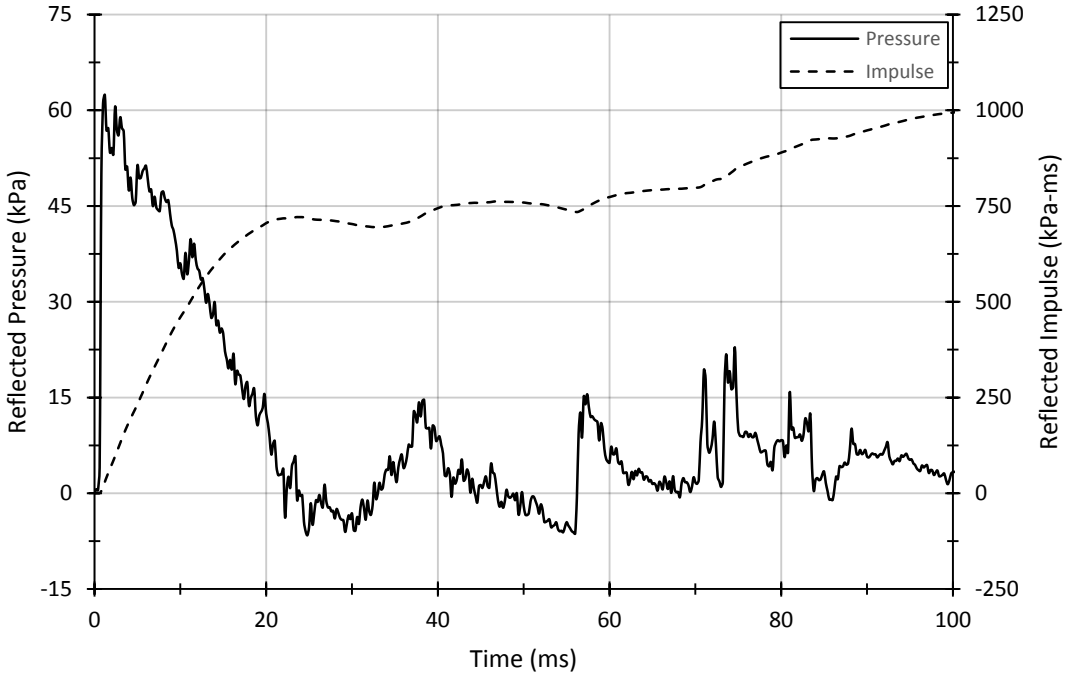

Figure A7.1: CLT 5-7 Pressure-Impulse Details

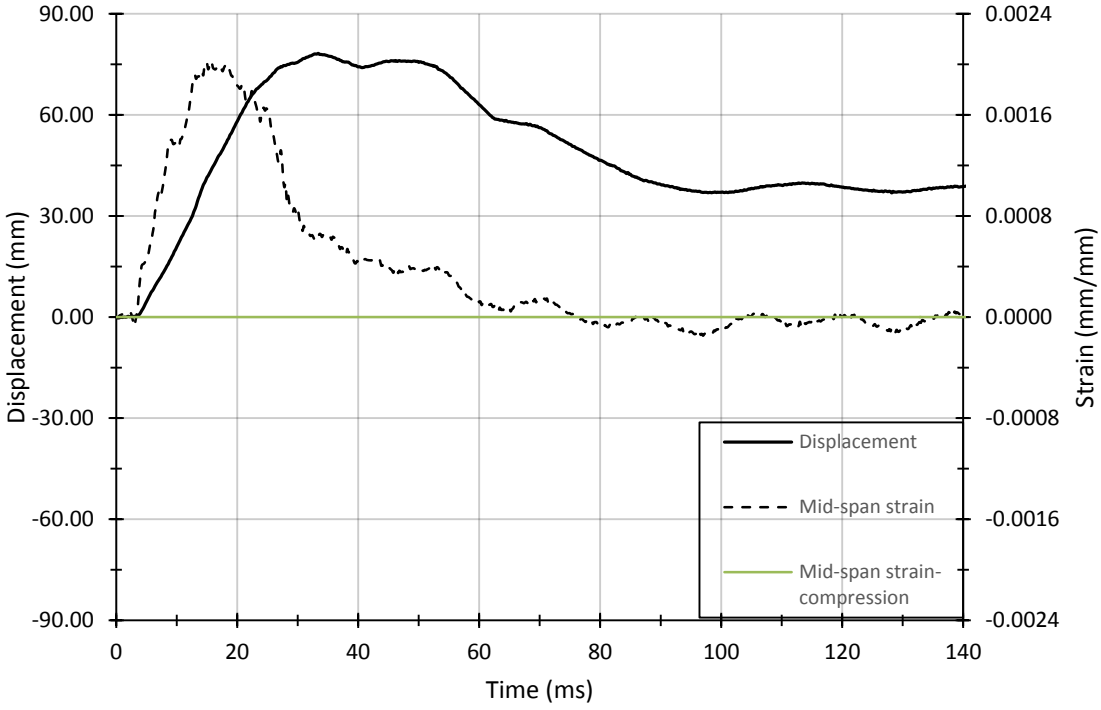

Figure A7.2: CLT 5-7 Strain and Displacement Details

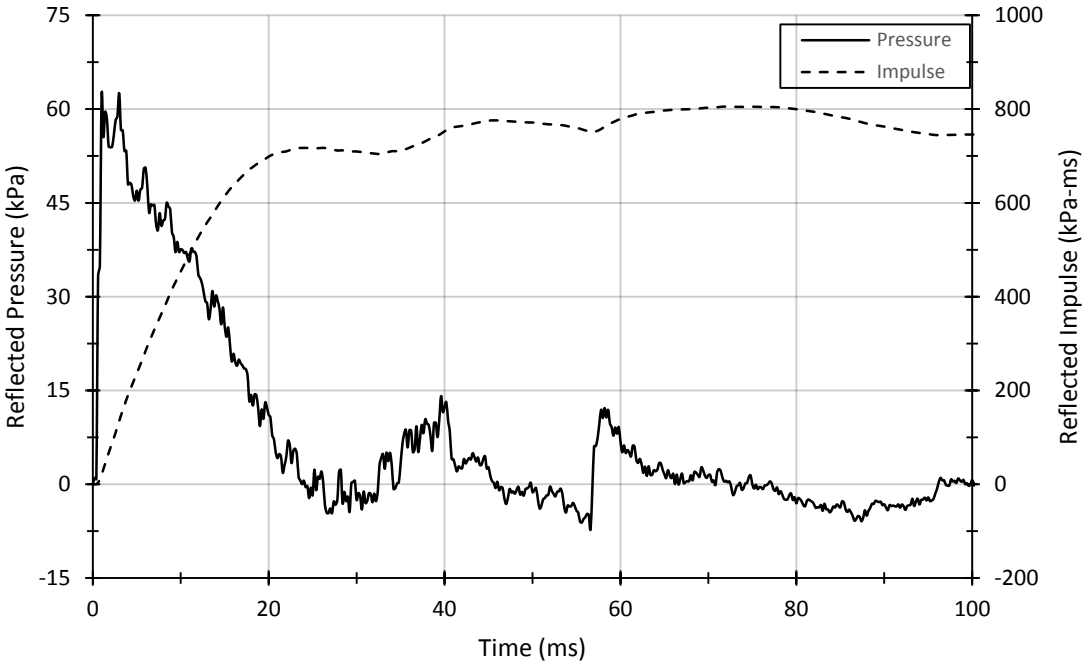

Figure A8.1: CLT 5-8 Pressure-Impulse Details

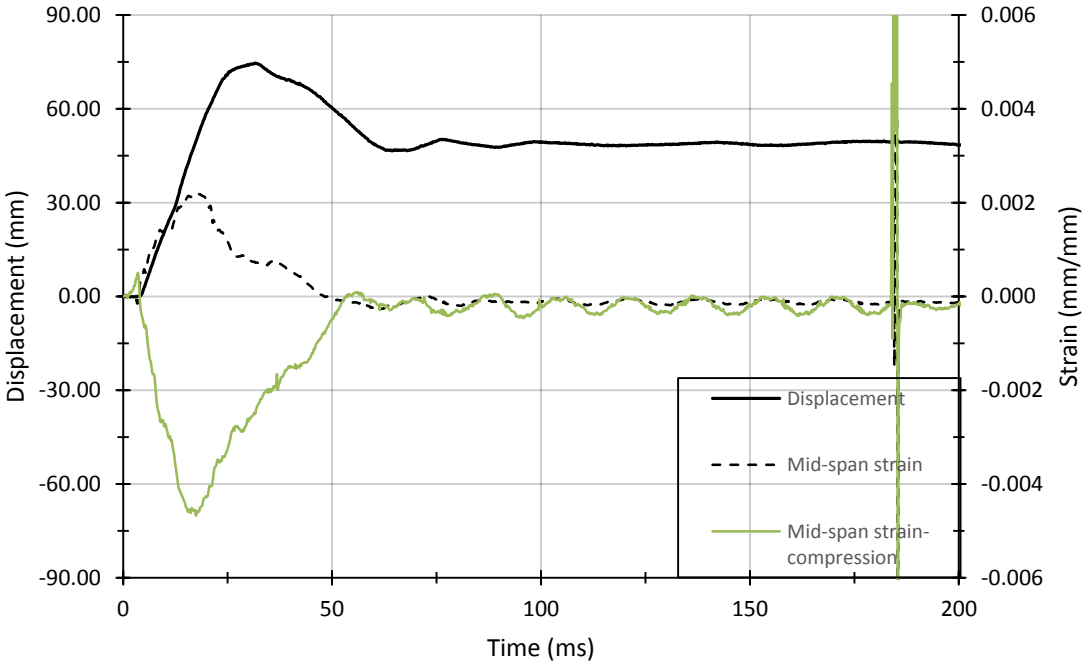

Figure A8.2: CLT 5-8 Strain and Displacement Details

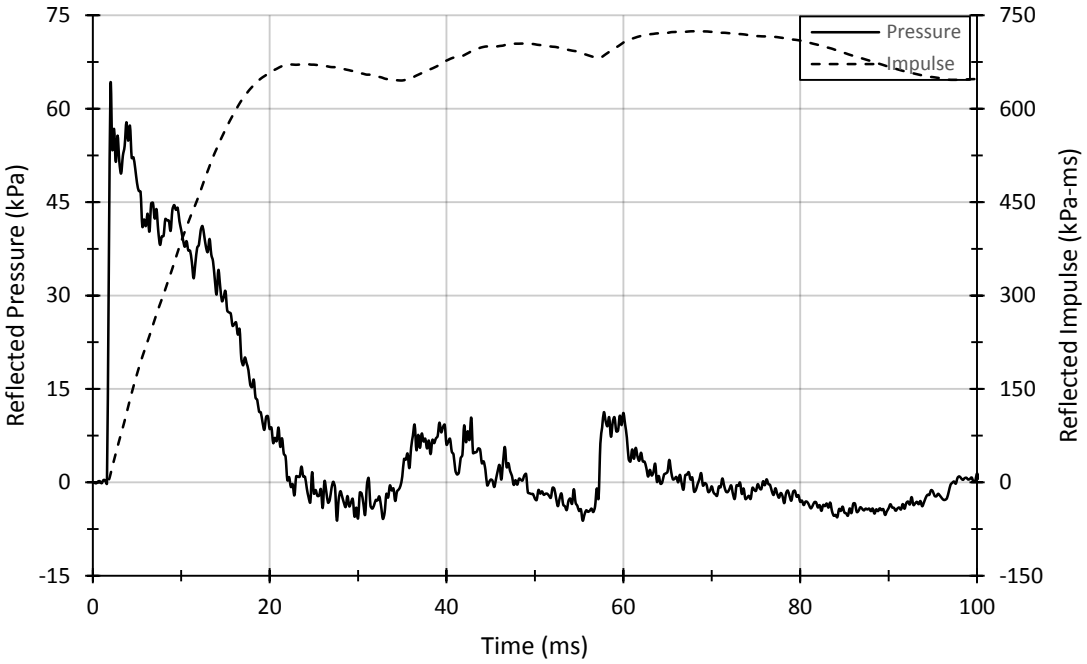

Figure A9.1: CLT 5-9 Pressure-Impulse Details

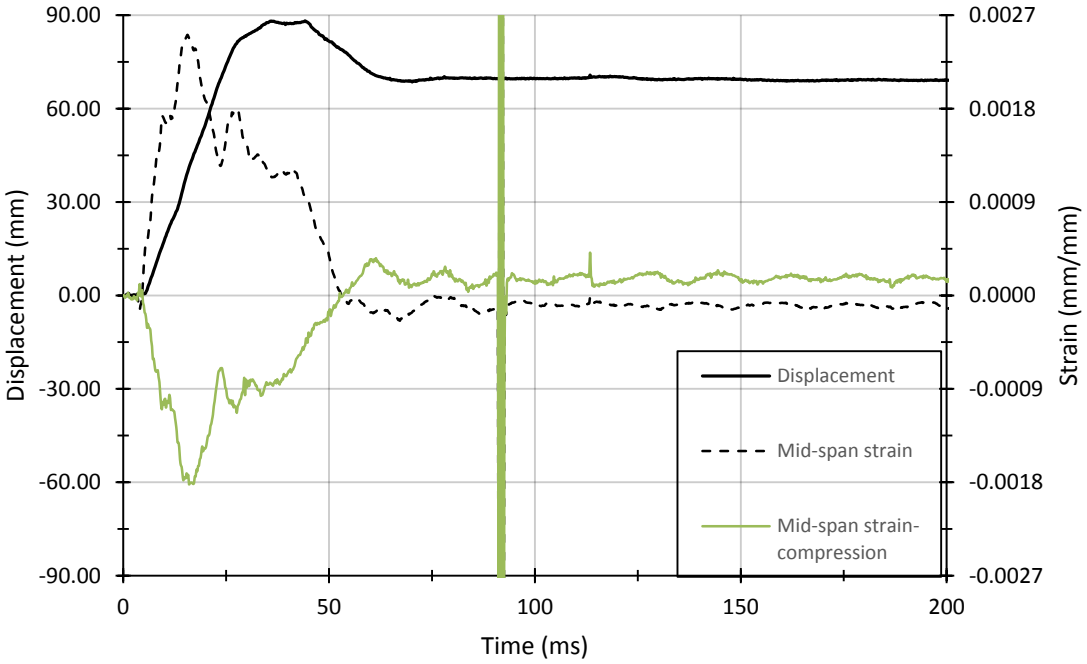

Figure A9.2: CLT 5-9 Strain and Displacement Details

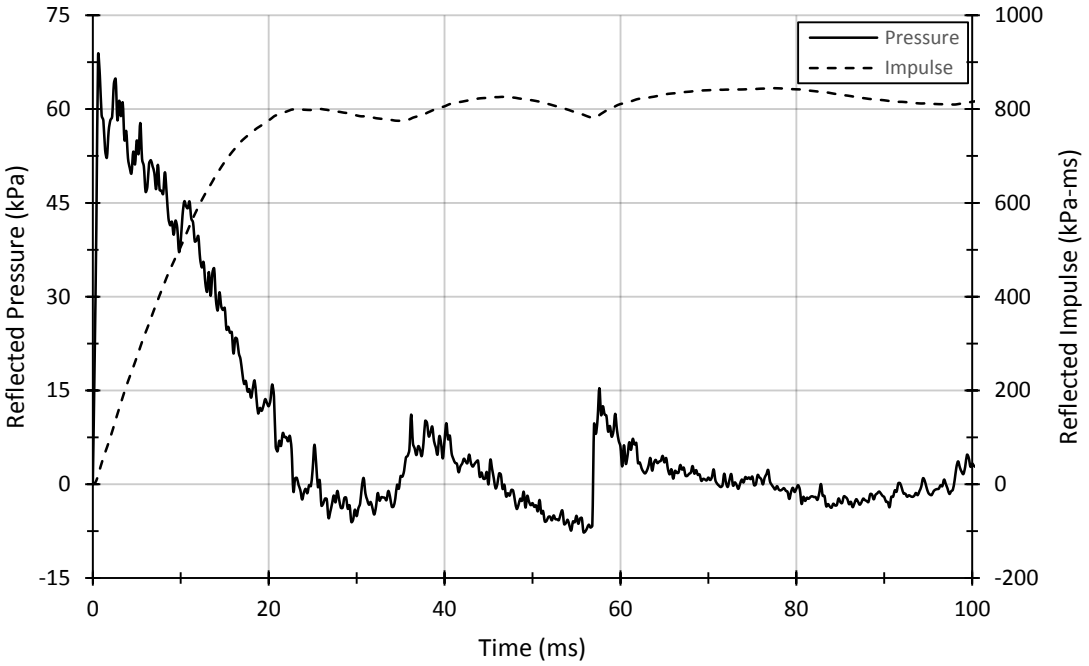

Figure A10.1: CLT 5-10 Pressure-Impulse Details

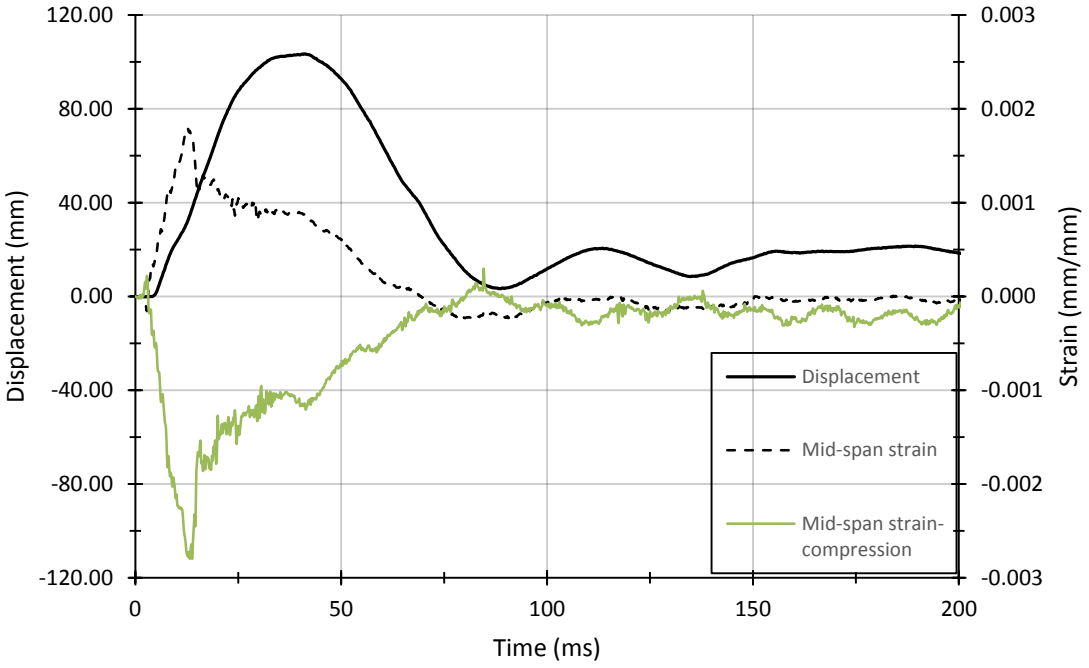

Figure A10.2: CLT 5-10 Strain and Displacement Details

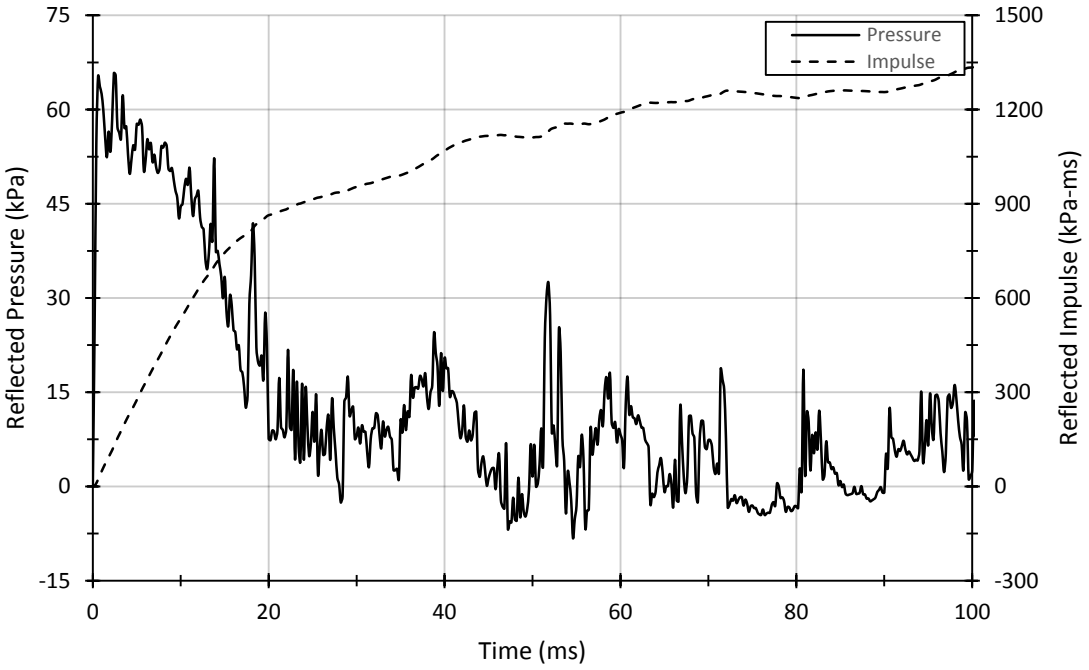

Figure A11.1: CLT 5-11 Pressure-Impulse Details

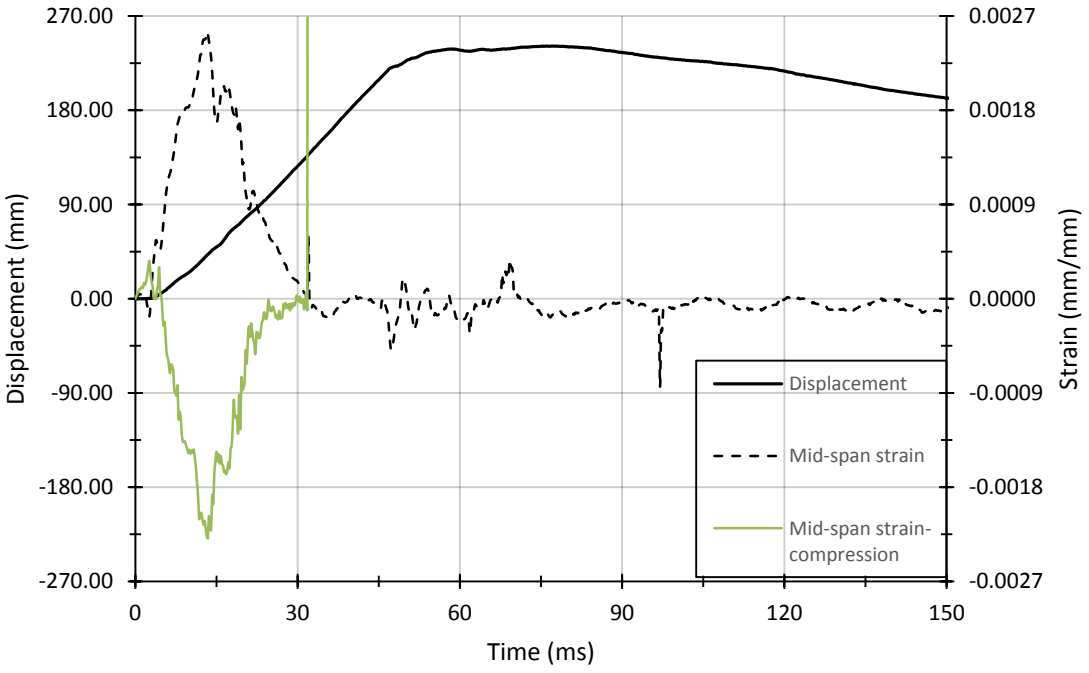

Figure A11.2: CLT 5-11 Strain and Displacement Details

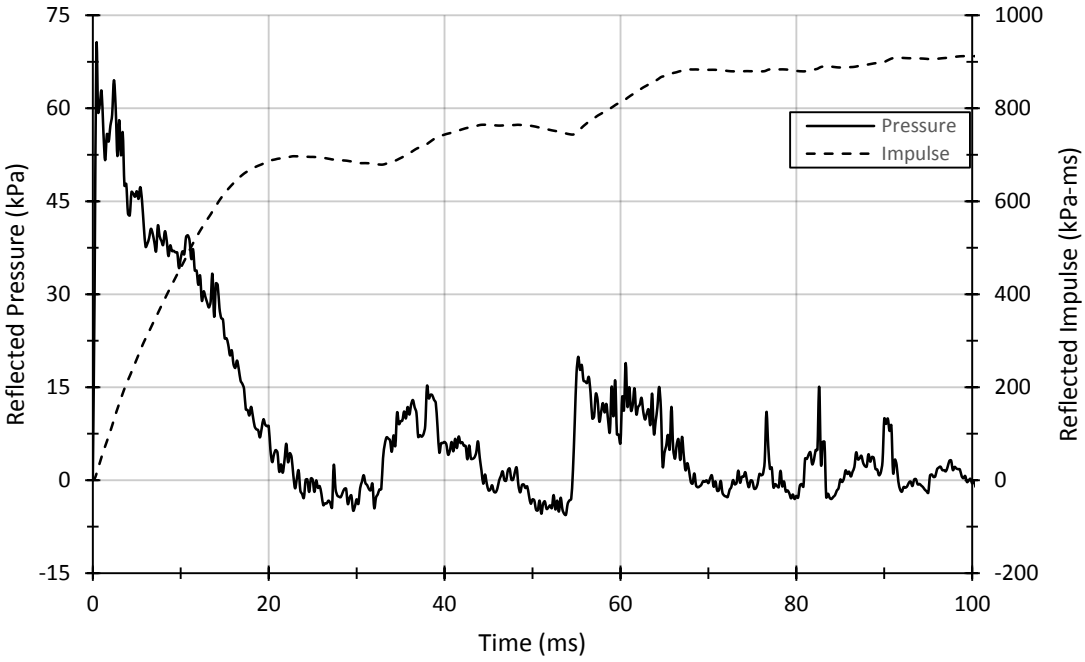

Figure A12.1: CLT 5-12 Pressure-Impulse Details

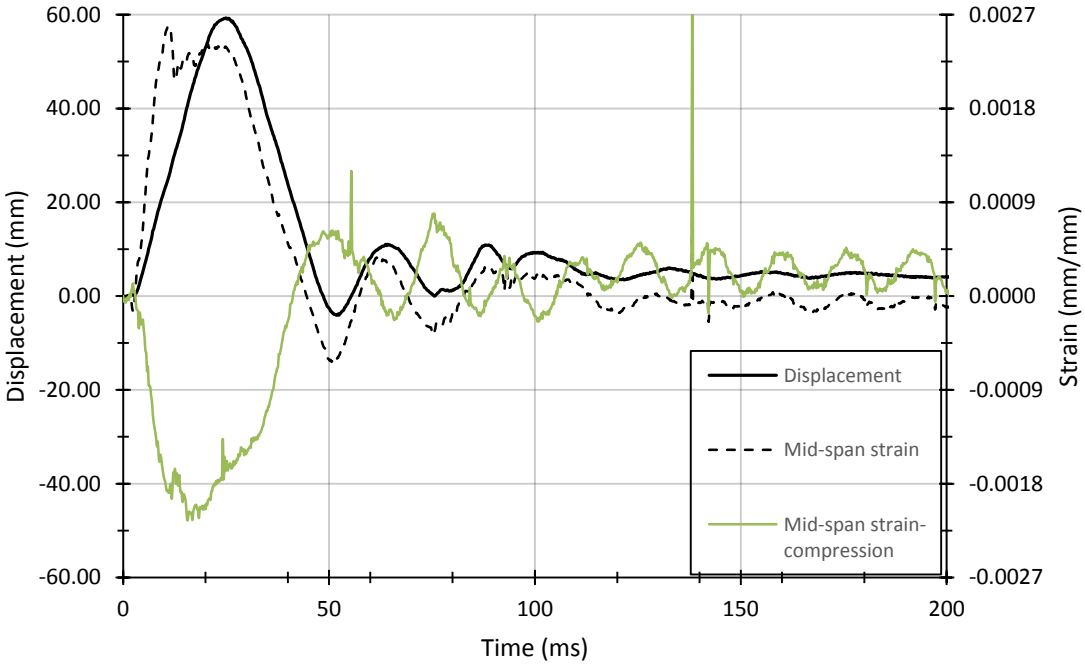

Figure A12.2: CLT 5-12 Strain and Displacement Details

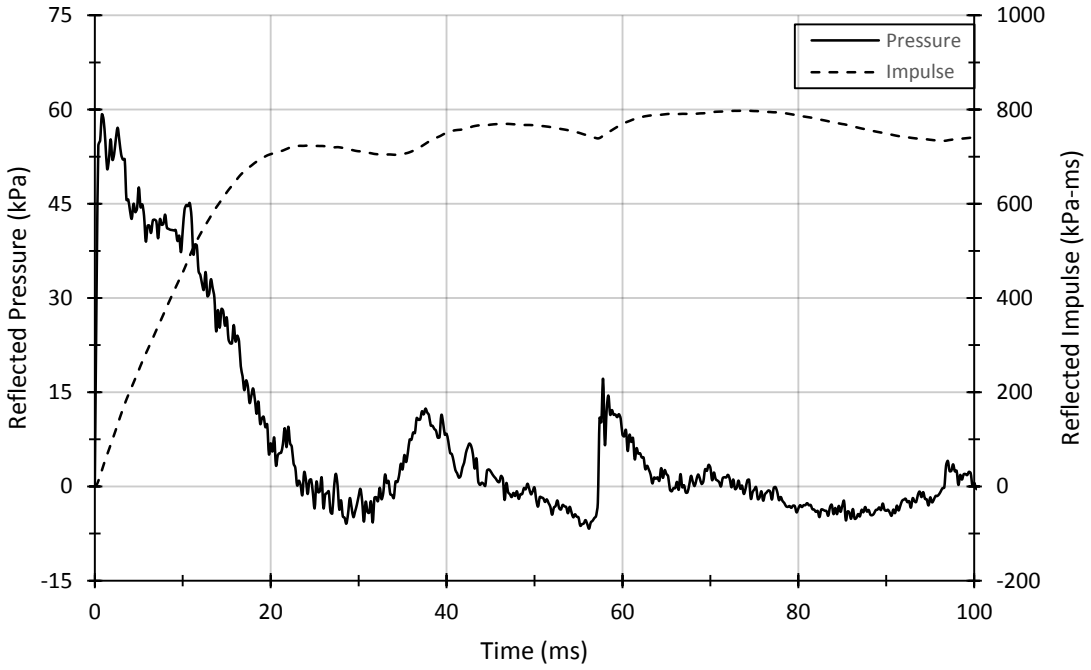

Figure A13.1: CLT 5-13 Pressure-Impulse Details

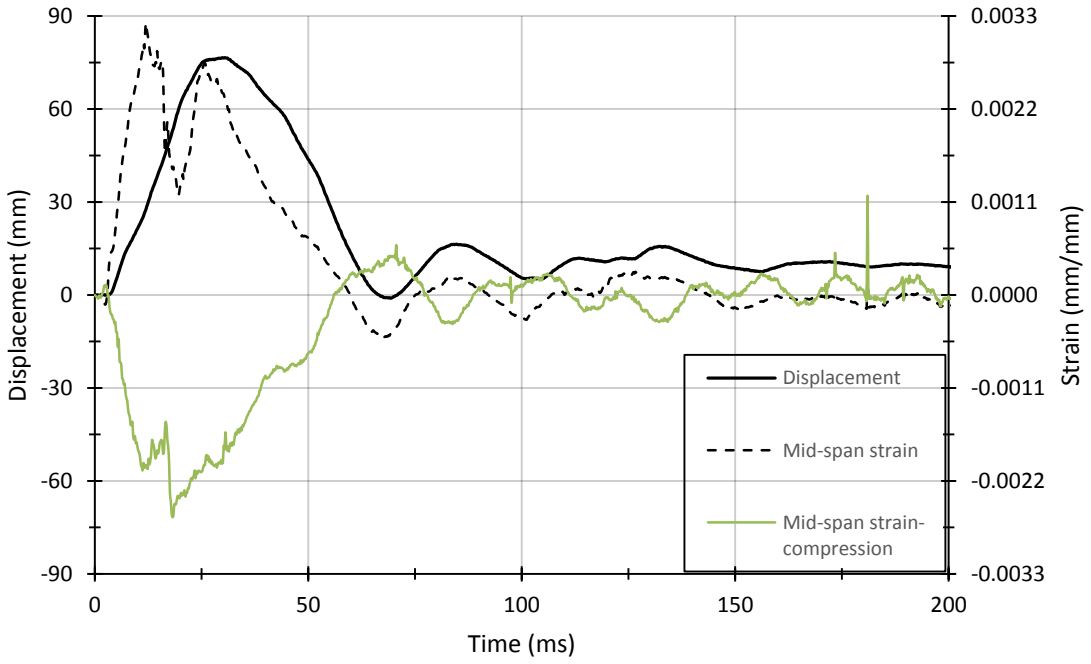

Figure A13.2: CLT 5-13 Strain and Displacement Details